THE ZEUS EXPERIMENT AT HERA.

Proposal 760

Bristol, Glasgow, Imperial College London, University College London, Oxford, Rutherford Appleton Laboratory
in collaboration with
Andrews, Argonne, Bologna, Bonn, Calabria, Chonnam, Columbia, DESY, DESY-Zeuthen, Florence, Freiburg, Hamburg, Jülich, Kazakhstan, KEK, Krakow, Kyungpook, Madrid, McGill, Moscow, NIKHEF, Ohio, Padova, Pennsylvania, Rome, Santa Cruz, Seoul, Siegen, Tel Aviv, Tokyo, Tokyo Metropolitan Univ., Torino, Toronto, Warsaw, Weizmann Inst., Wisconsin, Yale, York (Ontario).

1 Introduction

The upgrade to the HERA accelerator that will provide a five fold increase in luminosity and polarisation for the colliding beam experiments was carried out in 2001. Commissioning of the upgraded electron and proton rings began in August and first collisions were observed in the ZEUS interaction region in October. The commissioning of lepton beam polarisation will be performed at the start of running in 2002. High-luminosity e^+p running, with polarised positron beams, will begin at the end of January 2002. A two to three week shutdown is planned in April/May 2002 in order to switch from positron to electron beams. After a commissioning phase, it is planned that the machine will run with polarised electron beams for the rest of the year.

The ZEUS detector upgrade was also completed during the long shutdown in 2001. The silicon microvertex detector, in which the UK has a significant role, was completed, installed and commissioned and the forward tracking system was augmented with a straw tube tracker. The upgrade of the transverse polarimeter, where the UK has a leading role, was also completed.

The UK groups continue to make a strong contribution to both the preparations for data-taking and to data-taking itself. The UK provided both the 'pre-run' coordinator and his deputy and provide a good proportion of the shift leaders (4 units) and deputy shift leaders (2 units). The UK continues to take responsibility for a wide range of activities within the ZEUS collaboration: the ZEUS spokesman is a UK physicist; the UK provided the ZEUS tracking coordinator, the Monte Carlo code manager, the Monte Carlo coordinator, the CTD coordinator and the Straw tube tracker on-line expert; UK physicists are joint coordinators for three of the five ZEUS physics groups.

2 Central tracking detector status and infrastructure

The Central Tracking Detector (CTD) is a large-volume, cylindrical drift chamber covering the central region ($15° < \theta < 175°$). It provides charged-particle tracking, momentum measurement and identification through dE/dx. It also participates in all three levels of the ZEUS trigger.

The CTD's 4608 sense wires are arranged in nine superlayers, superlayer one being the innermost. The wires in odd-numbered superlayers run parallel to the chamber axis, whilst those in even-numbered layers have a small stereo angle ($\approx 5°$). Taken together they provide sufficient information to reconstruct tracks in three dimensions. All sense wires in the chamber are equipped with Flash Analogue-to-Digital Conversion (FADC) electronics and, in addition, all wires in superlayer one and the odd-numbered wires in superlayers three and five have z-by-timing electronics for the first-level trigger.

During the shutdown for the HERA upgrade the CTD was flushed with argon:CO_2. Despite not being operated for ten months, it successfully participated in cosmic tests for the ZEUS microvertex detector in July 2001.

2.1 Triggering

ZEUS operates a three-level trigger, of which the first is a hardware-based system whose principal aim is to reduce backgrounds that do not come from the interaction point. CTD information is essential for this and the detector uses dedicated, pipelined processor cards which provide tracking information to the global first-level trigger.

The ZEUS second-level trigger uses more precise software algorithms to clean the event sample further and classify certain types of physics events. Detail tracking information is provided by the CTD second-level trigger which makes use of the data from all five axial superlayers and the z-by-timing information from layers 1, 3 and 5. A precise measurement of the event vertex at the second level is a powerful technique for rejection of background. Before the shutdown for the HERA upgrade, modifications were made to the CTD Transputer network in order to allow data from the FADC electronics to be sent to the Global Tracking Trigger (GTT). This system will combine CTD data with the precise information from the new microvertex detector to provide a very accurate event vertex measurement. The link to the GTT computer systems has now been successfully tested.

The third-level trigger (TLT) runs on a farm of Unix workstations and PCs using an appropriate version of the off-line reconstruction code. The CTD TLT code is an optimised version of the full off-line reconstruction. Its performance is only slightly below that of the off-line version and aids monitoring of the system by providing early warning of any changes in critical CTD parameters.

2.2 Infrastructure and Monitoring

In general the CTD support infrastructure has performed very well. The CTD water cooling circuit is now fully operational again. A blocked pipe to the forward end plate was cleared by “sucking” the blockage out of the system. The water flow rates through both arms of the cooling system are now well above the minimum required to cool the CTD and show no signs of further fall off. Fine filters are also now installed between the main ZEUS cooling circuit and the input to the CTD water cooling system which it is hoped will prevent further problems.

The gas system operated reliably throughout the long HERA upgrade shutdown. After the cosmic tests some fluctuations in the gas composition were noticed. The problem was traced to a faulty mass flow controller, which has now been replaced with a new unit. The flow meters on the gas system have also been replaced as part of its ongoing maintainance.

New uninterruptable power supplies (UPS) have also been installed in the CTD high-voltage (HV) system. These new UPSs will provide increased protection from power failures and be more reliable than the previous units.

Since water was added to the gas mixture to overcome the Malter effect, as described in last year's report, the chamber has shown no further sign of HV instability. The addition of water caused some shift in the operating parameters of the CTD, including the reduction of the Lorentz angle to 41° from the nominal value of 45°. After some investigation it proved possible to restore this partially by reducing the CO_2 composition of the gas by 2% and increasing the ethane by 2% whilst keeping the argon constant, coupled with a small increase in the HV. The chamber is now operating efficiently once more and will continue to run with water in the gas mixture for the lifetime of ZEUS.

Over the course of the shutdown the ZEUS data-acquisition environment has been upgraded to operate with the larger data-rates expected in the post-upgrade environment. In particular, the ZEUS event-builder (EVB), a system that assembles the complete data for an event from all the sub-components of the detector, has been replaced with a new system. The CTD was one of the first components to move to the new EVB and is operating successfully with it.

ZEUS has implemented a system for automatic online data monitoring. For the CTD, this is done by checking a small number of critical histograms which are also made available to the shift crew. The automatic histogram checking was initially incorporated into the CTD online program, but will be moved to a dedicated machine in future for ease of maintenance and development. More detailed monitoring is performed off-line using samples of the data which are automatically analysed and then checked by a small team of experts. This system has proved to be effective over a number of years in the early diagnosis of problems. It also provides calibration constants for the CTD and quality control of the CTD data used for physics analysis.

The continued operation and reliability of the CTD is of utmost importance to ZEUS. The chamber is now ready for data-taking in the new HERA environment and will remain at the heart of ZEUS physics for the lifetime of the experiment.

3 ZEUS Microvertex Detector

ZEUS UK groups have been involved in the ZEUS MicroVertex Detector (MVD) project (mainly Oxford and UCL) with responsibility on the hardware side for: installation; clock and control electronics; the laser alignment system and a cable 'patchbox'. On the software side we wrote the local run control, event display and histogramming package, and are involved in the development of a second-level global track trigger We will also be involved in offline precision alignment using track data.

3.1 Clock and Control

The UCL ZEUS group provided the clock and control system for the MVD. This system consists of three main subsystems: a master controller and slave in the ADC crates; sixteen driver boards in a crate of their own; and twenty-four distribution cards in the patch boxes close to the detector, together with associated power supplies.

The master and slave system consists principally of digital logic on programmable devices. It (a) receives clock and trigger signals from the ZEUS global first level trigger (GFLT). (b) sends clock, trigger and reset signal to the HELIX driver system (c) receives busy and error signals from the ADCs and sends them to the GFLT. We also provided a ZEUS trigger simulator in the same crate as the master board, which allows standalone running. The master board also allows an external trigger to be input to the front panel, which was used durung cosmic ray data taking on the test stand.

The HELIX driver system (16 6U VME cards) fans out signals from the master and sends them as Low Voltage Differential Signals (LVDS) down approximately 20m of cable to the patch box cards. The system also interfaces with the MVD slow control to allow calibration data to be send to the detector chips at the start of a run, and provides monitoring information.

The patchbox cards consist of three cards for the control signals and three for the clock signals in each of the four patch boxes. These cards amplify the signals from the HELIX drvers and convert the control signal to single eneded CMOS signals as required by the HELIX chips. These cards formed part of what turned out to be the very challenging overall patchbox system (see below) and were designed by UCL and manufactured and installed by Oxford.

The whole system was delivered in time for cosmic ray testing in January 2001 in the test area, in which we participated, and is now fully installed and functional in the ZEUS hall.

3.2 Patchbox

The patchbox was not in the original proposal to the PPESP and did not sound too onerous ('just help with the design of a cable patch panel') when taken on. It turned out to be a major challenge and a key component on the critical path of the MVD project. Because of space limitations from existing components in ZEUS and the new magnets for the final focus, the nearest location for the main readout electronics was nearly 30m from the detector. Clearly a cable connection station was needed. Apart from very tight spatial limitations the design for what became known as the 'patch box' had to cope with:

- rearranging the cables from wafer-grouped on the MVD side to function-grouped (readout, clock & control, bias voltage, etc) on the readout side;
- rigorous screening of all MVD cables (high voltage, low voltage, clock and control, analogue readout) to avoid pickup in the hostile electronic environment near the beam line;
- active components to boost various the clock and control signals (see previous section).

A very ingenious design of doubly insulated crates with a specially designed back-plane was devised. To fit into the only space available around the rear beam-pipe the patch box was actually four separate boxes. The boxes were ready for the MVD 'full system test' at DESY (Dec 00 – Mar 01) and then had to be uncabled, moved to the ZEUS Hall, installed and recabled, with full testing of all MVD cables at each stage.

3.3 Alignment

The Oxford ZEUS group provided the laser alignment system [1] for the new microvertex detector. During regular operations the main purpose of the laser system will be to monitor gross movements of the MVD support structure with respect to the central tracking chamber. However the system proved its worth before and during the assembly of the MVD through 2000/01. Tests using part of the system at NIKHEF showed that the first design of the construction support frame was not rigid enough and needed strengthening. During assembly of the two halves of the MVD and their transport to DESY, periodic measurements were taken with laser system to monitor any distortions in the MVD cylindrical support tubes. Measurements were also taken before and after the delicate operation to put the two halves together at DESY prior to a full test of the MVD using cosmic rays and finally after installation of the MVD in ZEUS. VME alignment readout boards[1] are being constructed and will be installed in early 2002. At the same time the laser control system will be integrated into the MVD slow control system.

3.4 Installation

Installation was highly non-trivial because of space limitations and the delicate nature of the MVD. The procedures were worked out through extensive discussions with NIKHEF and DESY engineers and all the key stages were tested using various full-scale mock-ups. Apart from the challenge of getting the MVD into the central tube of the CTD with only mm clearance, the major problem was handling the 4m long readout and service cables attached to the MVD. These had to be fed in bundles through the CTD first. On the day everything worked perfectly and the MVD was installed by 6pm on 27/3/01. The final part of the installation was arranging the cables between the MVD and patch boxes in the very limited space around the new rear combined function magnet. This turned out to be a classic problem of fitting a round object (cables around the cylindrical magnet) into a square hole (aperture left when ZEUS rear calorimeter is closed).

[1]For the measurements to date, a prototype readout system with a limited number of channels has been used.

Although the cable routes and clearances had been checked very carefully beforehand, the first attempt failed and the calorimeter could not be closed completely. It turned out that certain drawings had not been completely accurate. The UK team had a weekend in which to try again and by using a simple wooden former and a lot of hard work managed to persuade the cables to take more rectangular profile thus allowing the calorimeter to close with a few mm spare.

3.5 Global Track Trigger

The Global Track Trigger (GTT) is a new trigger component for ZEUS. It is designed to combine the information from the existing, transputer based, readout systems for the CTD and STT with that from the new, VME based, readout system of the MVD as early as possible in the ZEUS trigger chain. Oxford and UCL are leading algorithm development and implementation. The GTT hardware consists of Gigabit ethernet communications and a farm of 12 1GHz Linux PCs for processing. This augments the original CTD second level transputer based system and has been funded through the Yale ZEUS group. The complete GTT system for integrating the CTD and MVD information is complete and has been tested within the ZEUS DAQ system. The algorithm for combining CTD and MVD information in the barrel region is ready for testing with the first real data. The STT[2] readout will be added before data taking in 2002 and work has begun on integrating the STT and forward MVD information into the existing algorithm. The performance of the algorithm has been studied extensively, using both Monte Carlo simulated events, pass though events taken during data taking last year, and cosmic muons taken during a short run in July this year.

In order to test the GTT latency performance before the availability of real e-p interaction data, a *playback system* has been created. Monte Carlo events stored in memory are injected into the GTT trigger chain at the component VME interfaces, and sent through the GTT system exactly as for normal data. Using simulated high-E_T dijet photoproduction events containing both MVD and CTD data, at an input rate of 400 Hz, the deadtime was found to be 1.4%, consistent with the performance of the existing ZEUS DAQ and trigger systems during data taking at the end of 2000.

The resolution performance of the algorithm with simulated MVD data has been studied for track and event vertex parameter reconstruction. The event vertex resolutions for the reference Monte Carlo sample are summarised in Table 1. The resolution of the GTT using CTD-only information is significantly better than the existing CTD SLT due to the use of the stereo information rather than the z-by-timing data. The improvement in the z-resolution of the primary interaction vertex will help to reduce background considerably and is also a necessary first step for more sophisticated trigger calculations, such as event track impact parameter distributions and/or secondary vertex algorithms.

	$\sigma_{z_{vtx}}$ (mm)
Current CTD-SLT	84.4
GTT (CTD Only)	11.3
Current Offline (no MVD)	1.14
GTT	0.046

Table 1: Event z_{vtx} resolution for GTT, existing CTD-SLT and existing offline reconstruction.

If the system performance and backgrounds are acceptable under real data taking conditions we hope to proceed with the inclusion of GTT based triggers using information on impact parameters and secondary vertices early next year. A nice summary of the status of the MVD

[2]A new forward Straw Tube Tracker, installed as part of the upgrade.

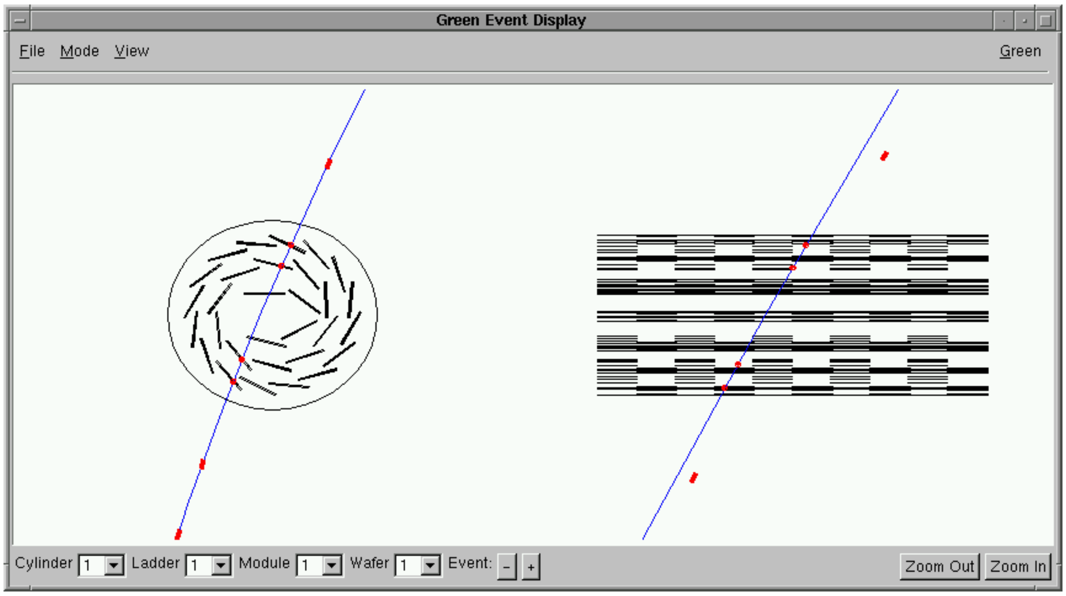

Figure 1: A cosmic ray track in the MVD, recorded during the system test, reconstructed using the GTT and display using the "Green" online event display.

project as a whole is given by Fig. 1, which shows a cosmic ray event, taken during the system test and reconstructed using the GTT software.

3.6 Online Software

The MVD run control, slow control and monitoring is carried out via a package based on the CERN ROOT software and known as 'Green'. This package includes histogramming and event display services (see figure 1) and was written by UCL. It has proved extremely flexible, and was used throughout the testing of the MVD. It is now fully integrated with the ZEUS global run control and will be used throughout data taking.

4 The HERA Polarimetry Upgrade

4.1 Overview

The polarisation dependence of the neutral current (NC) and charged current (CC) deep inelastic scattering (DIS) cross sections is a direct consequence of the chiral structure of the Standard Model, hence, measurements of these cross sections will allow imporant tests of the electroweak sector of the Standard Model to be made [2]. At present there are no measurements of CC DIS using polarised charged lepton beams and the data on the polarisation dependence of the NC DIS cross section is limitted to low Q^2. These measurements are now one of the primary objectives of the ZEUS collaboration.

4.2 Polarization Measurement at HERA

At HERA the lepton beam naturally becomes transversely polarised through the emission of synchrotron radiation, the Sokolov-Ternov effect. The transverse polarisation is converted into longitudinal polarisation at the interaction points using spin rotators, a series of magnets installed before and after the interaction point that cause precesion of the polarisation vector. At HERA, the polarisation, P, is measured independently by two polarimeters: TPOL – which measures the transverse polarisation; LPOL – which measures longitudinal polarisation. Each polarimeter shines a laser beam onto the lepton beam and detects the back scattered Compton photons. The laser photons are polarised; the polarisation state of the laser is alternately left- and right-circularly polarised. The LPOL measurement of the longitudinal polarisation relies on determining the energy asymmetry of the back-scattered photons between the left- and right-circular polarisations of the laser beam. The TPOL exploits the spatial, up-down, asymmetry. The polarised physics program at HERA requires that the polarisation must be measured with a precision ~1% and the upgrades to the LPOL and TPOL have been designed to meet this requirement. We are working on this as part of the cross-experiment POL2000 collaboration.

Members of the ZEUS UK collaboration have played a key role in the design, construction and commissioning of the silicon microstrip presampler upgrade to the TPOL. The upgraded TPOL consists of a calorimeter split horizonatally into an upper and a lower half instrumented with a silicon microstrip detector situated behind a one radiation length thick lead pre-radiator. The TPOL calorimeter measures both the total energy deposited by the Compton photons and the energy in the upper and lower halves of the calorimeter $E_{\rm up}$ and $E_{\rm down}$ respectively. The vertical, spatial, asymmetry is obtained from the $\eta - y$ transformation, where $\eta = (E_{\rm up} - E_{\rm down})/(E_{\rm up} + E_{\rm down})$, and y is the vertical coordinate of the photon impact point on the calorimeter face. The role of the silicon microstrip detector is to determine the $\eta - y$ transformation precisely in situ and in real time. The back-scattered Compton photon beam is highly intense and of very small extent. Hence, in order to guard against possible differential radiation damage a single scintillating fiber mounted on a precision stage is used to monitor the linearity of the response of the silicon microstrip detector. TPOL has been instrumented with two silicon microstrip detector planes. The first, the y-sensor, has 768 horizontal strips and measures the y-coordinate. The second, the x-sensor, has vertical strips. The x-sensor is used to centre the TPOL in the Compton photon beam precisely. The scintillating fibre system (scintillating fibre, photo-detectors, readout and associated software) is the responsibility of other ZEUS members of the POL2000 collaboration.

4.3 Silicon Detector for the TPOL

A prototype silicon detector was tested successfully at the begining of 2001 in a test-beam at DESY. The prototype setup consisted of 1×1 cm^2, 80 μm pitch silicon sensor, the TPOL calorimeter, and a prototype scintillating fiber detector. We were able to demonstrate a signal to noise ratio of ~ 20, an efficiency of 97% and the expected position resolution. With the experience gained, we manufactured the first iteration of the 6.3×6.3 cm^2, 80 μm pitch detector front-end board for the y-sensor. This detector was tested at test-beams at DESY and at CERN in July and August 2001 together with the TPOL calorimeter and the final scintillating fibre system. A summary of the results obtained is shown in figure 2. Data analysis is still in progress so that these results should be regarded as preliminary. Figure 2a shows the linearity of the response of the calorimeter when exposed to positrons with energies ranging from 6 GeV to 40 GeV. A relative non-linearity of better than 1% has been achieved. The energy resolution of the calorimeter is shown in figure 2b. A fit to the data yields a resolution of $\sigma_E/E \simeq 25\%/\sqrt{E} \oplus 4\%$. Figure 2c shows the $\eta - y$ correlation as measured using a 10 GeV positron beam at CERN. The $\eta - y$ transformation derived from the 1996 CERN Test is also shown for comparison. Finally, the performance of the scintillating fibre system is shown in figure 2d. The y-coordinate reconstructed in the silicon for events with signals in the fibre is plotted against the vertical position of the fibre. The residuals to a straight line fit are shown in the inset. The width of the residual distribution is better than 50 μm. The excellent results obtained over the summer demonstrate that the upgraded TPOL gives the required performance under test-beam conditions.

The first iteration of the x-sensor, a 6.3×6.3 cm^2, 120 μm pitch silicon microstrip detector was completed in October 2001. The full silicon detector system was tested successfully at DESY and the upgraded TPOL was installed in the HERA tunnel at the end of November.

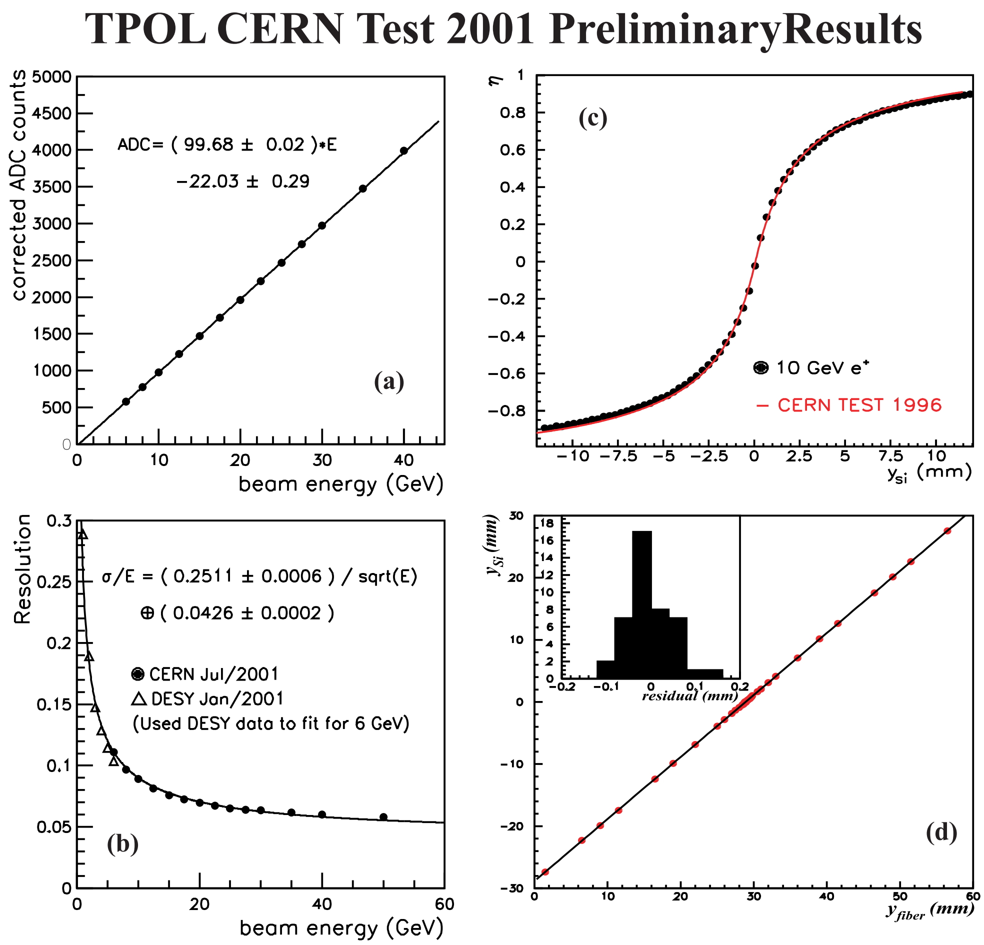

Figure 2: Summary of test-beam results obtained at DESY and at CERN over the summer of 2001. (a) the linearity of the response of the calorimeter when exposed to positrons. (b) calorimeter energy resolution determined using electron and positron beams. (c) $\eta - y$ correlation measured using a 10 GeV positron beam (points). The $\eta - y$ transformation derived from the 1996 CERN Test is shown as the solid line. (d) The y-coordinate reconstructed in the silicon for events with signals in the fibre is plotted against the vertical position of the fibre. The residuals to a straight line fit are shown in the inset.

Analysis of the CERN and DESY test beam data showed that the $\sim 9\%$ of the strips on the y-sensor are dead. This is undesirable, but the performance of the y-sensor (see Fig. 2) still meets the requirements. At present the cause of this high fraction of dead strips is believed to lie in the kapton foil pitch adapter used for the first iteration front-end boards. In addition, one of the two readout chips used on the x-plane does not respond to signals from the sensor while performing as expected in response to test pulses. The causes of the problems encountered in both the x- and the y-sensors are still under investigation. We plan to put in place an improved quality control system to ensure that the production of the final iteration of the front-end boards do not suffer such failures.

The temperature in the HERA tunnel can be as high as 35 °C. We therefore plan to cool the detector and have tested a water based chiller system during running in the DESY test-beam. Analysis of the temperature data is underway and will allow us to specify the chiller power required. We expect to install the cooling system along with the final iteration of the front-end boards early in 2002.

5 Physics analyses

During 2001 eleven ZEUS analyses were published or submitted for publication to various journals, of which three were originally submitted in 2000. In this section, we concentrate as usual on those physics areas where the UK members of ZEUS have been particularly active.

5.1 High Q^2 Neutral, Charged Current Physics and Structure Function Measurements

5.1.1 High-Q^2 neutral current physics

Within the framework of the Standard Model, neutral current deep inelastic scattering is mediated by the exchange of a photon or a Z between the incoming lepton and the proton. The cross section for NC scattering is given by

$$\frac{d^2\sigma_{\rm NC}^{e^{\pm}p}}{dxdQ^2} = \frac{2\pi\alpha^2}{xQ^4}[Y_+F_2(x,Q^2) - y^2F_L(x,Q^2) \mp Y_-xF_3(x,Q^2)] \quad (1)$$

where Q^2 is the negative of the 4-momentum transfer squared between the lepton and the proton, x is the Bjorken scaling variable, y is given by $Q^2 = sxy$ and $Y_{\pm} = 1 \pm (1-y)^2$. The parity violating cross section xF_3, is expected to become significant at large Q^2.
ZEUS UK physicists have continued their leading role in studies of high-Q^2 physics at HERA. The determination of the NC cross section from the 16 pb^{-1} of e^-p data collected in 1998 and 1999 is nearing publication. In September 1999 HERA switched to e^+p collisions and ZEUS collected 64 pb^{-1} of data up to June 2000. Fig. 3 shows the NC differential cross section $d\sigma/dQ^2$ for both electron and positron beams at a centre-of-mass energy of 320 GeV. For $Q^2 > 3\,000\,\text{GeV}^2$ the e^-p cross section is observed to lie above the e^+p cross section. The SM prediction gives a good description of the data. Figure 4 shows $d\sigma/dx$ for $Q^2 > 10\,000\,\text{GeV}^2$ for both e^+p and e^-p at ($\sqrt{s} = 320$) GeV along with the SM predictions. The e^-p cross section lies above the e^+p cross section and the SM prediction gives a good description of the data. Within the SM the fact that the e^-p NC DIS cross section is larger than the e^+p cross section at high Q^2 is attributed to the fact that for e^-p NC DIS the interference between the photon- and the Z-exchange contribution is constructive while for e^+p NC DIS it is destructive.
The reduced cross section $\tilde{\sigma}_{\rm NC}^{e^{\pm}p}$, where

$$\tilde{\sigma}_{\rm NC}^{e^{\pm}p} = \frac{1}{Y_+}c\frac{xQ^4}{2\pi\alpha^2}\frac{d^2\sigma_{NC}^{e^{\pm}p}}{dxdQ^2}, \quad (2)$$

is shown at fixed x as a function of Q^2 in figure 5. For Q^2 values above $1\,000\,\text{GeV}^2$ the e^-p cross section lies above the e^+p cross section; consistent with the SM expectation. The structure function xF_3 has been extracted by combining the e^-p data with the e^+p data collected in 1996 and 1997. The precision of the measurement is comparable with the first extraction of F_2 from the data taken in 1992. This measurement will benefit from the increased data from the high luminosity running which is soon to commence. An improved measurement of xF_3 will impose a tighter constraint on the high-x valence quark distribution which plays an important role in estimating very high energy processes at the LHC. In addition, the measurement of the dependence of the neutral current cross sections on the charge and polarisation of the lepton beam will be sensitive to the electroweak couplings of the light quarks.

5.1.2 High-Q^2 charged current physics

In charged current deep inelastic scattering the exchanged W-boson picks out specific quark flavours from within the proton. Thus e^+p CC DIS is sensitive to the d valence quark density at

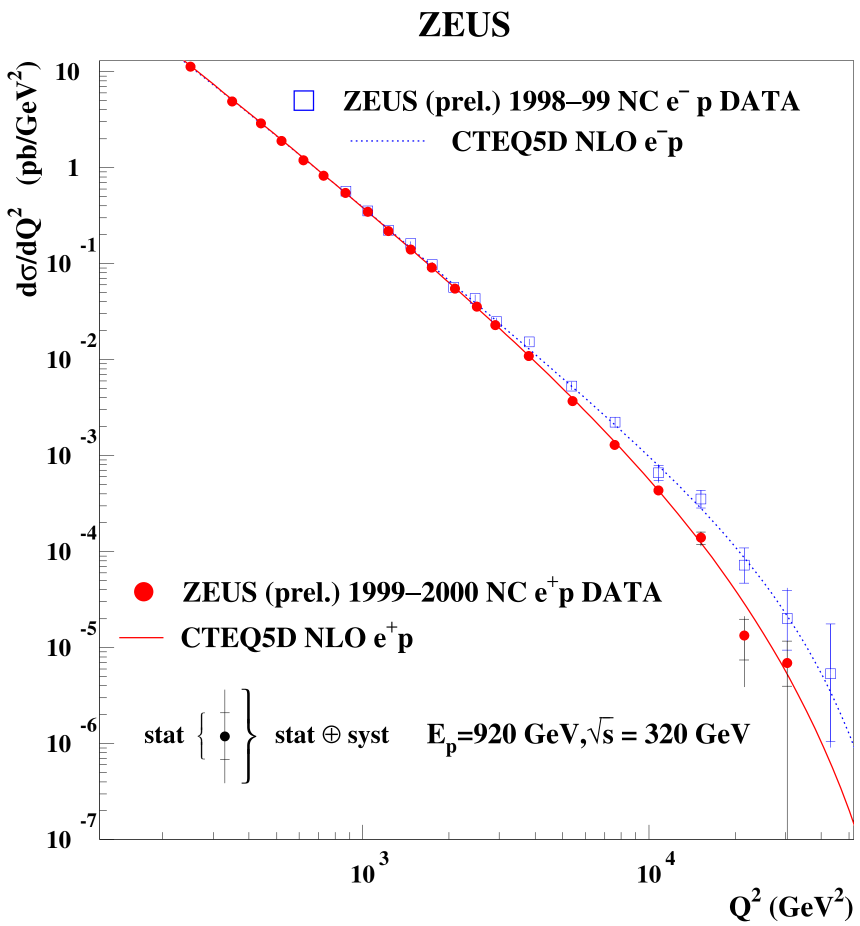

Figure 3: Differential e^+p and e^-p $d\sigma/dQ^2$ cross sections compared to the Standard Model predictions from CTEQ5D (solid line).

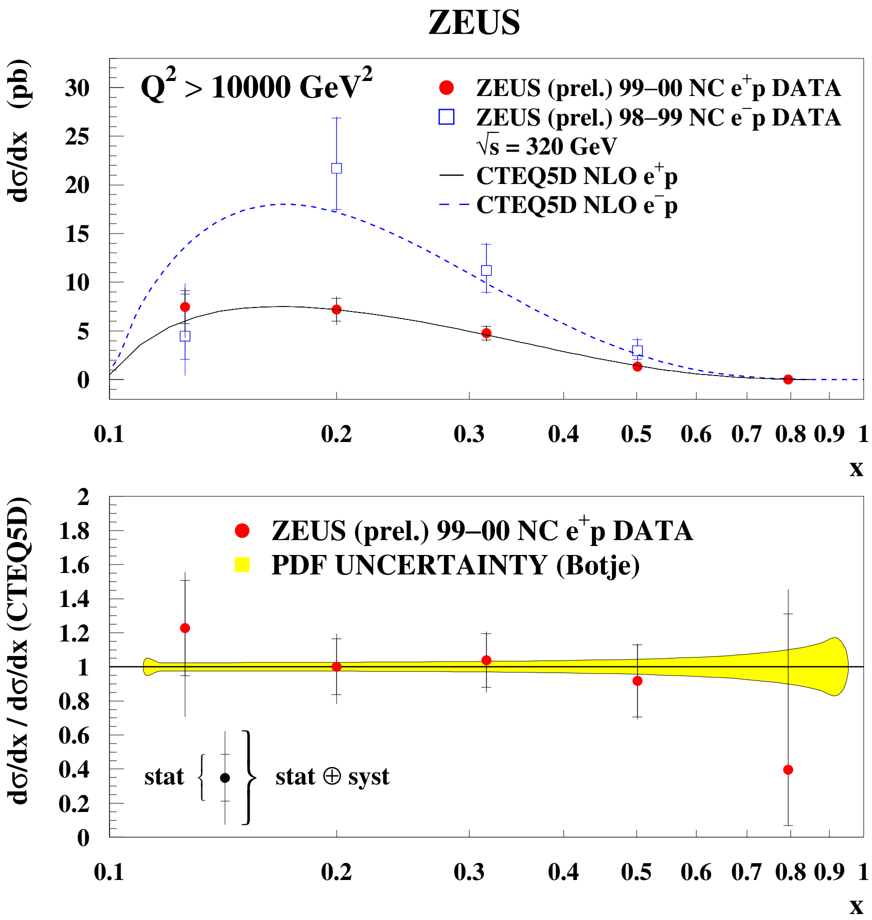

Figure 4: Differential e^+p and e^-p $d\sigma/dx$ cross section for $Q^2 > 10\,000\,\mathrm{GeV}^2$ Standard Model predictions from CTEQ5D. The lower plot shows the ratio of the ZEUS measurement to the Standard Model prediction. The shaded band shows the uncertainties associated with the PDFs.

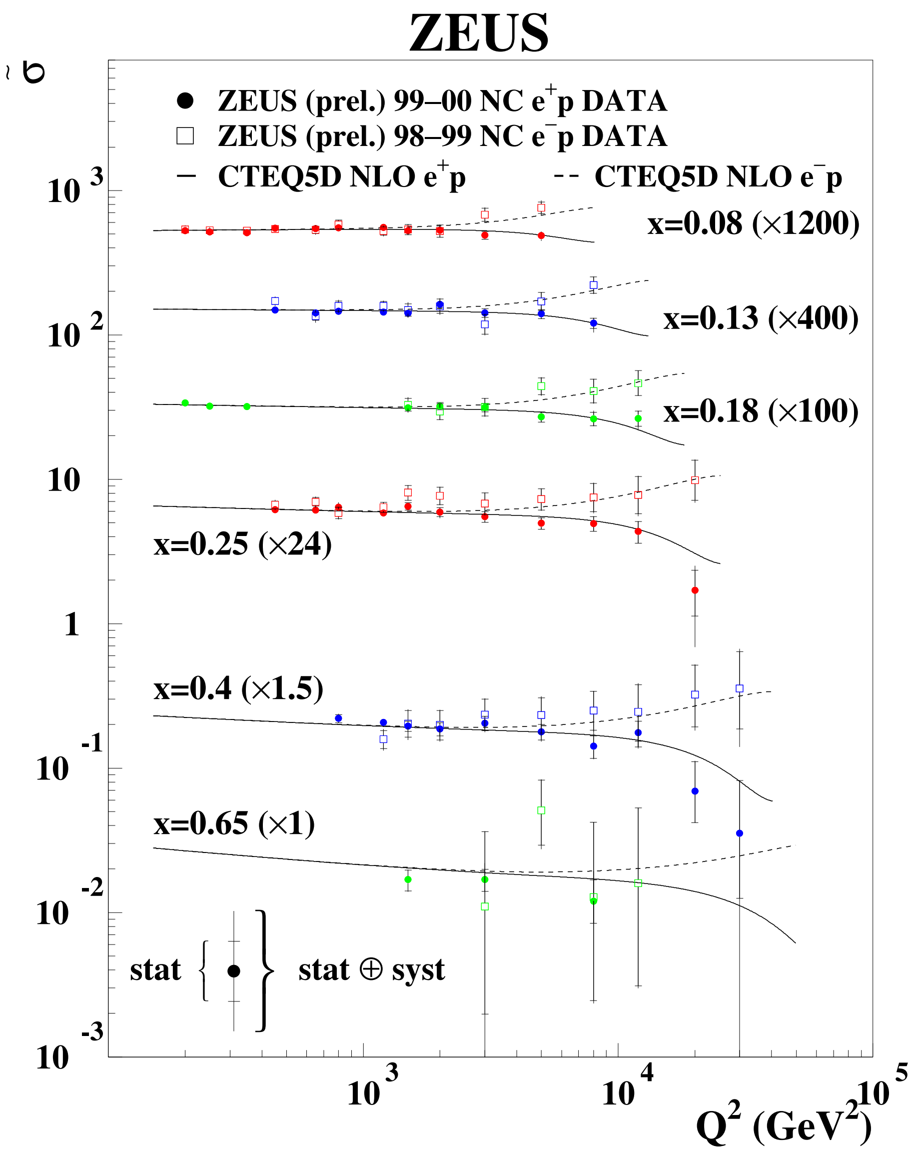

Figure 5: The reduced e^-p and e^+p cross sections compared to the Standard Model predictions from CTEQ5D. For $x > 0.18$, the e^-p data is seen to rise at high values of Q^2, as opposed to the e^+p data which turns down at large values of Q^2.

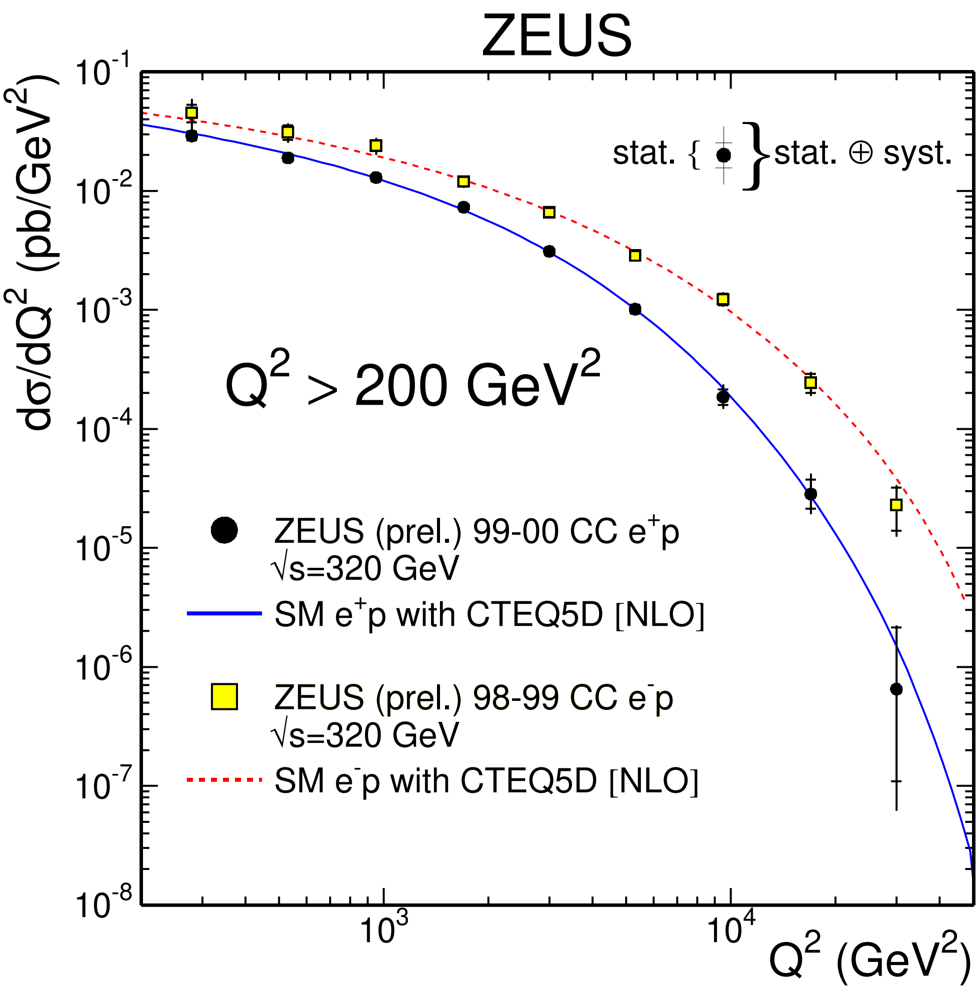

Figure 6: The CC DIS Born cross section, $d\sigma/dQ^2$, for e^-p data (squares) and e^+p data (filled circles). The dashed and solid lines show the Standard Model expectation evaluated using the CTEQ5D PDFs for e^-p and e^+p scattering, respectively.

high x and the $\bar{u}$ (and $\bar{c}$) quark density at low x. In contrast, e^-p CC DIS is sensitive to the u valence quark density at high x and the $\bar{d}$ (and $\bar{s}$) quark density at low x. Hence by measuring the dependence of the CC DIS cross section on the charge of the lepton beam we are able to study flavour-specific parton densities directly.

The analysis of the 16 pb^{-1} of e^-p data taken during 1998 and 1999 is now complete and a publication is expected in the very near future. The analysis of the e^+p data taken in 1999 and 2000 is nearing completion, preliminary results were shown at conferences in 2001. Fig. 6 shows the cross section $d\sigma/dQ^2$ for both e^-p and e^+p scattering. The e^-p cross section is higher than that of e^+p at all values of Q^2, rising to a factor greater than 10 at the highest Q^2 measured. In the quark parton model, this is understood to be due to the W coupling to the higher u-quark density in e^-p scattering, while the dominant e^+p process is the W coupling to d-quarks with a $(1-y)^2$ suppression. The Standard Model expectation, evaluated with the CTEQ5D parton density functions (PDFs) gives a good description of the data.

Fig. 7a shows the cross section $d\sigma/dx$ for $Q^2 > 200$ GeV^2, the ratio of the measured cross section to the SM expectation is shown in Fig. 7b. The SM, evaluated with the CTEQ5D PDFs, gives a good description of the cross section over the full range of x. The double differential CC cross section may be written as

$$\frac{d^2\sigma^{CC}}{dx\,dQ^2} = \frac{G_F^2}{2\pi x}\left(\frac{M_W^2}{M_W^2+Q^2}\right)^2 \tilde{\sigma}_{\rm CC}^{e^\pm p} \tag{3}$$

where the e^-p reduced cross section, $\tilde{\sigma}_{\rm CC}^{e^\pm p}$, is given at leading order in QCD by $\tilde{\sigma} = u + c + (1-y)^2(\bar{d}+\bar{s})$ (for e^+p, change quarks to anti-quarks and vice versa). The reduced cross section, for both e^-p and e^+p, is plotted as a function of x at several fixed values of Q^2 in figure 8. The Standard Model, evaluated with the CTEQ5D PDFs, gives a good description of the data.

5.1.3 Structure Functions

ZEUS UK groups continue to be strongly involved in the measurement and analysis of structure functions. The high precision F_2 measurement using data taken in 1996 and 1997 was published this year [3]. Fig. 9 shows this data as a function of Q^2 at fixed x. Since the statistical precision of the data is $\lesssim 1\%$ (over the range $2.7 < Q^2 < 800$ GeV^2) a detailed evaluation of systematic errors has been performed and a systematic uncertainty of $\sim 3\%$ has been achieved over much of the kinematic range. ZEUS data now have comparable precision to fixed target structure function measurements and have vastly extended the kinematic range of precision structure function measurements.

The UK has also played a leading role in the interpretation of the new high precision data by preforming NLO QCD fits, using the DGLAP formalism, to determine the parton density functions (PDFs) and $\alpha_{\rm S}$. The increased range ($6.3\times10^{-5} < x < 0.65$, $2.7 < Q^2 < 3\,0000$ GeV^2) and the high precision of the data allow a much improved determination of the structure function F_L, the gluon and the sea-quark distributions compared to our previous work [4]. The parton distributions extracted from this fit are shown in Fig. 10 for $Q^2 = 10$ GeV^2. The error bands take full account of uncertainties from correlated experimental systematic errors. The fit predicts that at low Q^2 ($Q^2 \sim 1$ GeV^2) the $q\bar{q}$-sea distribution is still rising at small x, whereas the extracted gluon distribution is suppressed. This is incompatible with the hypothesis that the rapid rise of F_2 is driven by the rapid increase in gluon density at small x through $g \to q\bar{q}$ splitting. The new precision data exhibit these trends more strongly than the previous data set, and will allow us to come to more definite conclusions regarding the lower Q^2 limit of validity of the NLO QCD DGLAP formalism. If the fit is extrapolated back into the kinematic region of the precise ZEUS BPT 1997 data [5] it is clear that the fit is unable to describe the data for $Q^2 \le 0.65$ GeV^2.

The fit can also determine the value of $\alpha_{\rm S}$ taking full account of the correlations between the shape of the parton distribution functions and α_S, giving

$$\alpha_{\rm S} = 0.1172 \pm 0.0008({\rm stat+uncorr}) \pm 0.0054({\rm corr}), \tag{4}$$

where the first error represents statistical and uncorrelated systematic errors and the second error represents the correlated systematic uncertainties from all the contributing experiments (including normalization uncertainties).

The ZEUS data are crucial in determining the gluon and the sea distributions but they also have some impact on the valence distributions. A fit can be made to ZEUS data alone if the high Q^2 e^+p CC DIS cross-section data are included [6]. This fit produces a larger d valence distribution at high x than the standard fit which includes fixed target data, but there is no disagreement at the current level of statistical precision of the CC data. The forthcoming high-luminosity running will allow us to significantly extend these studies.

The longitundinal structure function, F_L, arises from QCD corrections to the parton model. A measurement of F_L is therefore important as it directly probes the gluon density. The key to making such a measurement is to obtain a dataset in which a range of values in y can be accessed at the same values of x and Q^2. Members of ZEUS UK have developed an analysis which makes

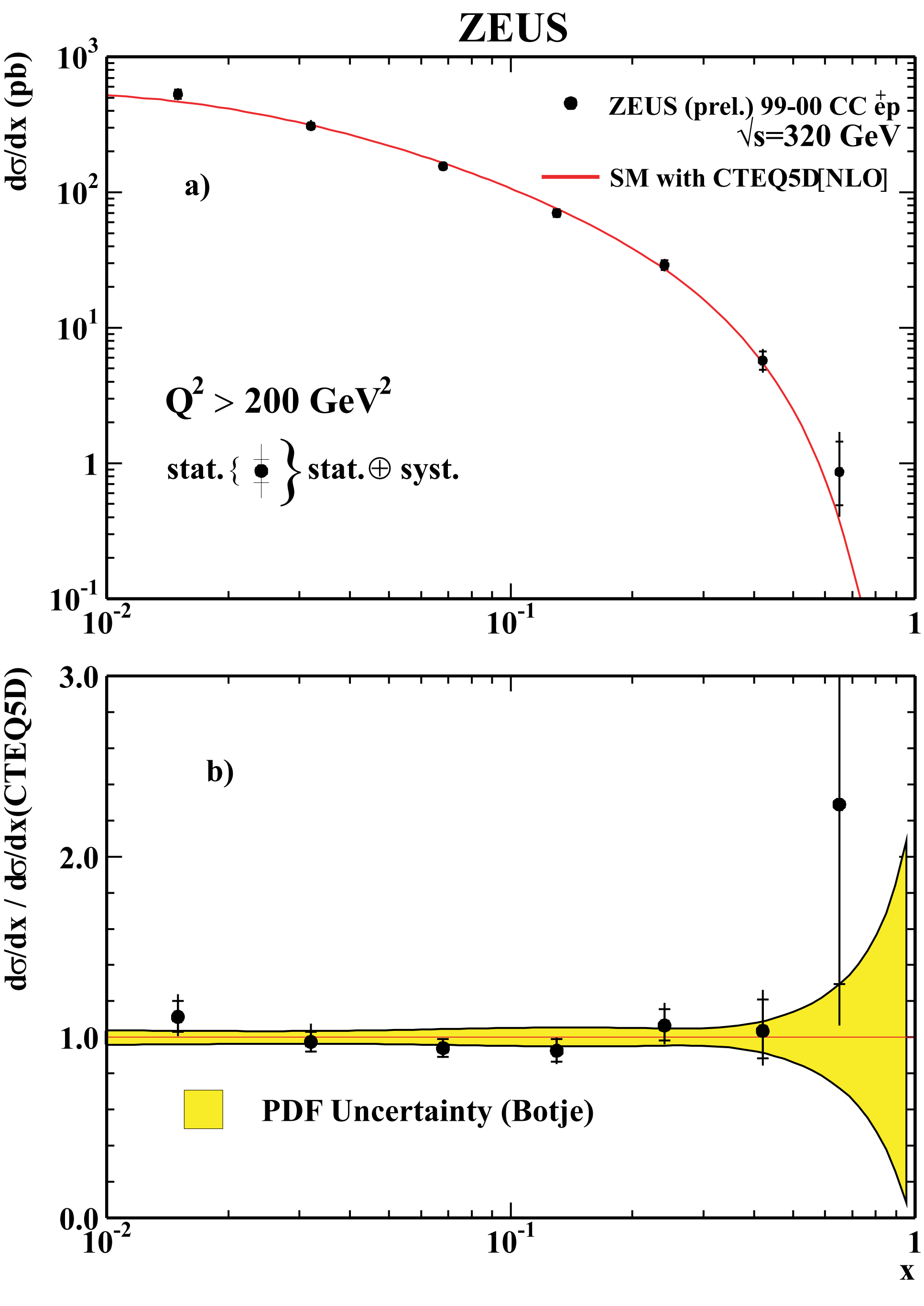

Figure 7: (a) The CC DIS Born cross section, $d\sigma/dx$ (filled circles). The solid lines shows the Standard Model expectation evaluated using the CTEQ5D PDFs. (b) The ratio of the measured cross section to the SM expectation evaluated using CTEQ5D PDFs. The shaded band shows the uncertainties associated with the PDFs.

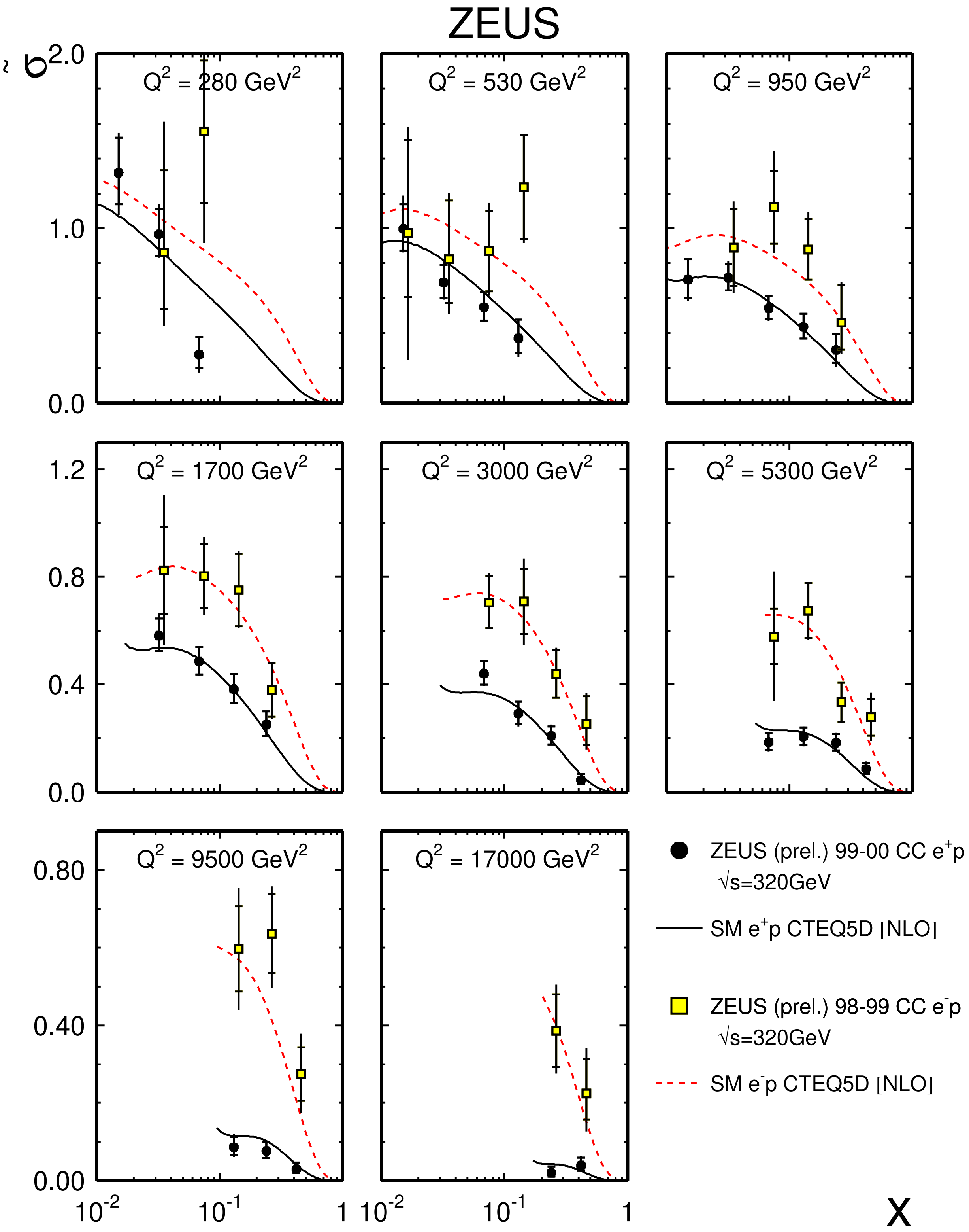

Figure 8: The reduced cross section, $\tilde{\sigma}$, as a function of x, for different fixed values of Q^2. The squares and filled circles represent the e^-p and e^+p data respectively, while the expectations of the Standard Model evaluated using the CTEQ5D PDFs are shown as the dashed and solid lines.

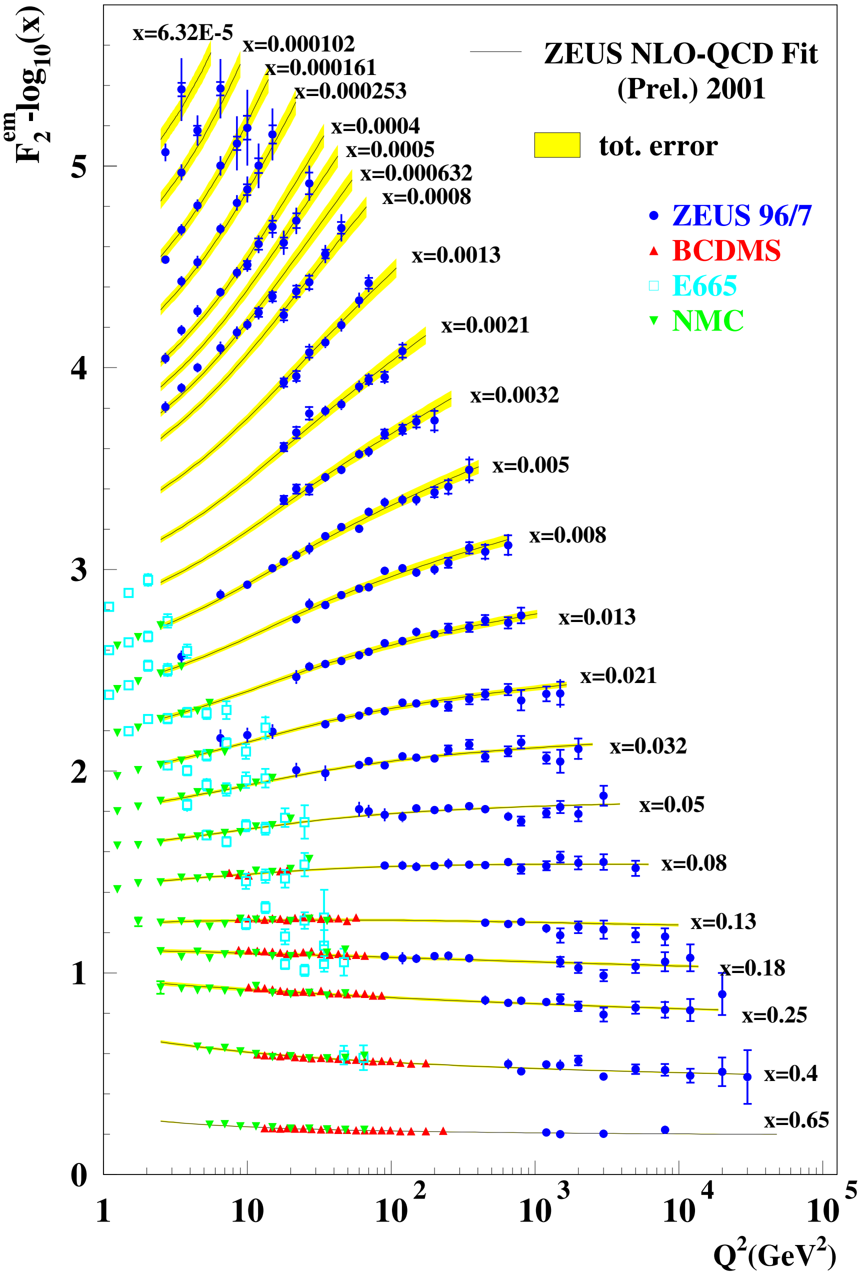

Figure 9: ZEUS 96/7 F_2 data and fixed target data compared to the ZEUS NLOQCDfit

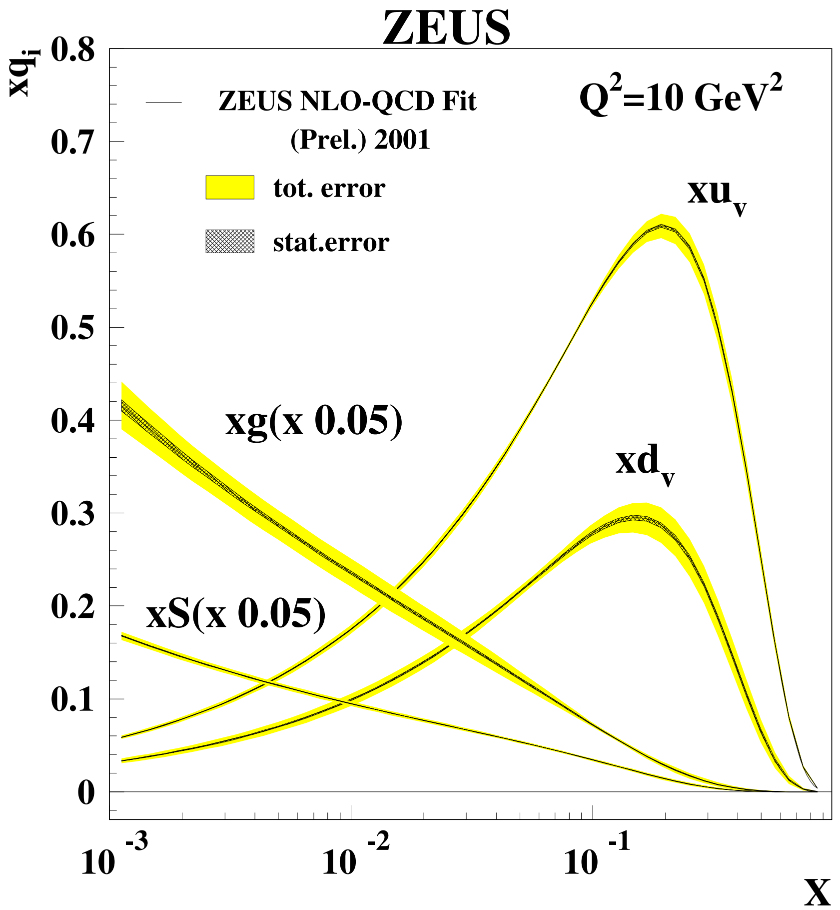

Figure 10: The glue, sea, u and d valence distributions extracted from the standard ZEUS fit, at $Q^2 = 10\text{GeV}^2$, with the error bands resulting from statistical, uncorrelated and correlated systematic errors.

use of initial state radiation (ISR) to vary the effective centre of mass energy and consequently to vary y at fixed x and Q^2. The analysis is technically complicated. To date, F_2 has been determined using the ISR technique from data collected in 1996. The good agreement between the value obtained and the published F_2 gives confidence in the method. An initial extraction of F_L has been performed and the results obtained look promising. We expect to develop the analysis for publication during 2002.

5.2 Heavy quark production

ZEUS UK groups have been involved in many aspects of the programme to undertand heavy quark production, both in data analysis and hardware and software aspects. Analyses investigating the production rate and nature of beauty and charm quarks are making significant contributions in a field which is still poorly understood. The production of charm quarks in DIS and accompanied by jets in photoproduction are now being measured precisely. This is discussed below along with the first measurement of open beauty production at ZEUS. Details of the ongoing hardware and software projects which will aid in the detection of heavy quarks are discussed in Section 3.5.

5.2.1 Charm production in DIS

Heavy quarks, particularly charm, are produced copiously in DIS, predominantly via the boson-gluon fusion process. This means that measurements of charm production allow, in principle, a direct determination of the gluon density in the proton. Charm has traditionally be identified by two decay chains, $D^{*+} \to D^0\pi^+$, $D^0 \to K^-\pi^+$ or $D^0 \to K^-\pi^-\pi^+\pi^+$ which have low backgrounds but also have small branching ratios. Using a luminosity of 37 pb^{-1}, ZEUS has published a measurement of charm production via these two decay channels [7]. Predictions of NLO QCD describe the data well over the full range in Q^2. The gluon distribution in the proton used was determined from fits to inclusive measurements of the proton struture function, F_2^p. The consistency of this prediction with the charm data demonstrates the universality of the gluon distribution in the proton, independent of the final state. Using all currently available ZEUS data along with other decay channels will greatly improve the precision of these measurements. UK physicists are taking a leading rôle in both of these directions. Very high-statistics measurements of heavy quark production in DIS will be a major goal with the new data to come with the upgraded HERA accelerator and ZEUS experiment.

5.2.2 Charm production with jets

With the larger statistical sample in the photoproduction regime ($Q^2 < 1$ GeV^2), charm production accompanied by jets, is providing a detailed picture of many aspects of QCD and, in particular, the charm content of the photon. The first measurement of charm quarks inside jets was published in 1999 [8], with UK physicists as principal authors. The results showed for the first time that charm is produced copiously in resolved-photon events. Building on these results, resolved-photon processes have been studied further in order to understand if the charm quark is an active parton in the photon or produced only in the hard scatter.
In charm events where two jets are produced, measurements of the angle, θ^*, between the jet-jet axis and beam direction in the dijet rest frame allow the dominant propagator in the hard scatter to be determined. Events in which the photon acts as a pointlike object (boson-gluon fusion) have a quark propagator; the cross section as a function of $|\cos\theta^*|$ is therefore $\propto (1-|\cos\theta^*|)^{-1}$. In contrast events with a gluon propagator have a cross section which is $\propto (1-|\cos\theta^*|)^{-2}$. If charm were not active in the photon, then charm in resolved-photon processes would be produced only

via gluon-gluon fusion which has a quark as the propagator. Events enriched in direct- or resolved-photon processes can be selected by requiring $x_\gamma^{OBS} > 0.75$ and $x_\gamma^{OBS} < 0.75$, respectively; the variable x_γ^{OBS} is the fraction of the photon's momentum taking part in the production of the two jets of highest transverse energy. Figure 11 shows the measured $\cos\theta^*$ distribution in the two regions of x_γ^{OBS}. The measurement is based on a luminosity 119 pb^{-1}, almost all of the avaliable pre-upgrade data. For $x_\gamma^{OBS} > 0.75$, the data show a shallow rise consistent with events having a quark propagator, whereas for $x_\gamma^{OBS} < 0.75$, the data show a more rapid rise to high $\cos\theta^*$, consistent with the dominance of a gluon propagator. Resolved-photon events with a gluon propagator can only arise if the charm is active in the photon ($Q_\gamma g_P \to Qg$). The data are adequately described by predictions from the Pythia MC simulation and provides the strongest evidence so far of a heavy quark density in the photon.

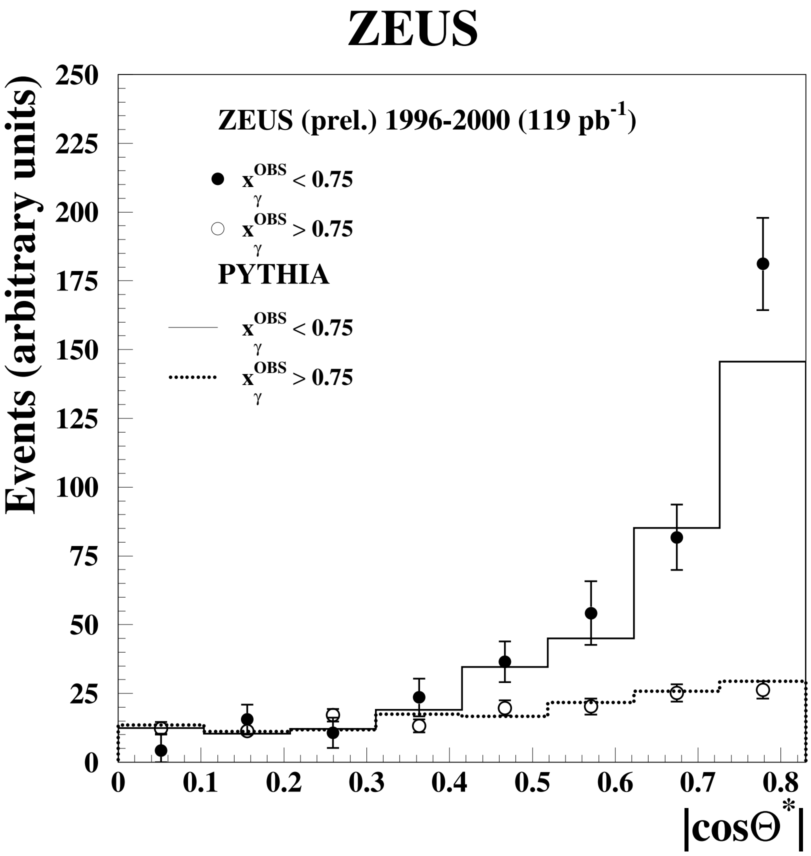

Figure 11: The $\cos\theta^*$ distribution in charm-tagged events for $x_\gamma^{OBS} > 0.75$ and $x_\gamma^{OBS} < 0.75$. Predictions from the Pythia MC are compared to the data.

Also investigating the nature of the photon in charm events, the evolution of its structure with virtuality, Q^2, has been measured. The measurement is again using a luminosity of over 100 pb^{-1}. It has been observed in inclusive dijet events that the ratio, $\sigma(x_\gamma^{OBS} < 0.75)/\sigma(x_\gamma^{OBS} > 0.75)$ falls with Q^2, indicating the suppression of resolved-photon events with increasing photon virtuality. Figure 12 shows the ratio $\sigma(x_\gamma^{OBS} < 0.75)/\sigma(x_\gamma^{OBS} > 0.75)$ for dijet events accompanied by a charm quark tagged by reconstructing D^* mesons. The data is compared to various leading order Monte Carlo models. In Figure 12(a), models in which the partonic content of the photon is both suppressed and has no suppression as a function of Q^2 is compared to the data. Both models adequately describe the features of the measurement. Comparisons of models with no explicit resolved-photon component are made in Fig. 12(b). The Aroma model, which implements the

DGLAP evolution scheme, lies below the data. The CASCADE model, which implements a version of the CCFM evolution scheme, gives a good description of the data.

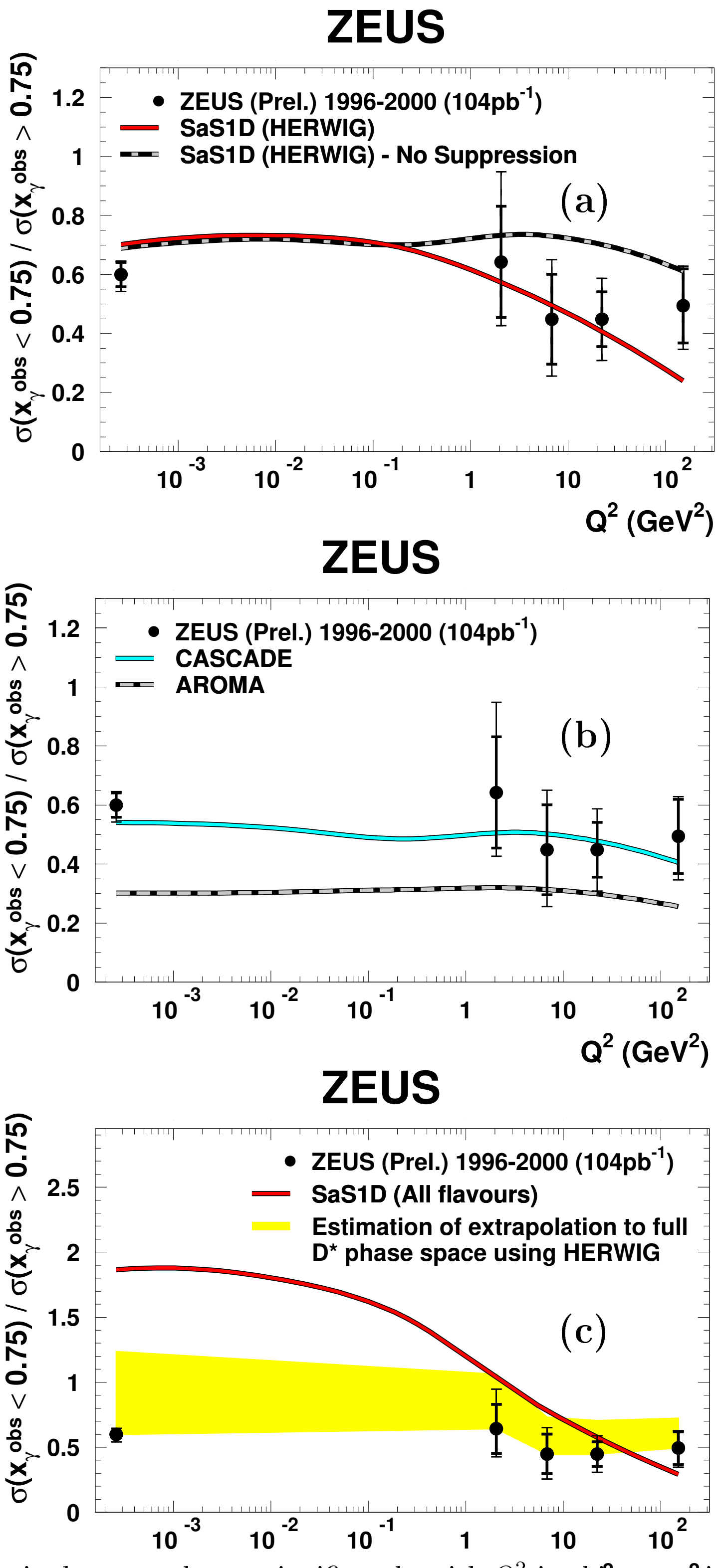

The fact that the ratio does not change significantly with Q^2 in this range is in marked contrast to the case in which the charm requirement is not made, and suggests that the suppression of the low-x_γ^{OBS} cross section due to charm and the suppression due to photon virtuality are not independent. This has been quantified by extrapolating the measurement to the full kinematic

Figure 12: Ratio of low to high x_γ^{OBS} for events with a D^* meson compared to (a) the SaS1D photon structure functions, (b) the AROMA and CASCADE MC models. In (c), the data is extrapolated to the full phase space of the D^* meson and compared to the SaS1D photon structure function.

range of the $D^{*\pm}$ meson. The extrapolation is shown in Fig. 12(c) and demonstrates that the ratio falls off more slowly in the presence of charm than it does when charm is not required.

5.2.3 Beauty production

Heavy quarks can also be detected by identifying electrons from their decay. This is done by measuring the distinctive rate of energy loss of electrons in the CTD, as well as the way they interact in the calorimeter. Results by UK physicists from this method show a significant production rate for beauty quarks as can be seen in figure 13. The beauty component is identified by measuring the transverse momentum of the electron relative to the jet axis since electrons from beauty decays are expected to have a harder p_T^{rel} spectrum owing to the mass of the b. The beauty fraction has been extracted by fitting the data distribution with Monte Carlo. The measurements were published in 2001 [9]

Existing measurements of open beauty production from HERA, $\gamma\gamma$ collisions at LEP and $p\bar{p}$ colliders show cross sections that are high when compared to standard NLO QCD predictions. A direct comparison of the ZEUS result with an NLO QCD prediction is also possible by using the Monte Carlo to extrapolate to the $b\bar{b}$ cross section in a limited kinematic region. This extrapolated cross section is shown in Fig. 14; it also lies above the theoretical prediction.

Understanding such results is an important test of QCD and a necessary step towards understanding the new physics potential of future colliders. The results also represent a substantial technical triumph in the operation and understanding of the CTD dE/dx readout, a UK responsibility from the beginning of ZEUS.

The presence of heavy quarks in the evolution of the photon structure offers a promising window for understanding the development of QCD structure, splitting functions and threshold effects. The ability at HERA to select concurrently on jet transverse energy, $E_T^{\rm jet}$, photon virtuality and x_γ^{OBS}, as well as to compare heavy flavour jets with untagged jets, makes it uniquely suitable for detailed studies in this area. Thus heavy flavour jet production will be a growth area, and is a major driving force behind the UK's involvement in the MVD. The GTT will play a vital part in allowing these events to be saved at relatively low $E_T^{\rm jet}$ even after the upgrade, particularly if charm enrichment can be implemented.

5.2.4 Charm Production in Diffractive Scattering

The study of charm production in diffractive scattering is a crucial part of the investigation of the diffractive process and the underlying mechanism responsible for diffraction. This is because charm production occurs predominantly in gluon-driven interactions and the models make substantially different predictions for the behaviour of gluons in diffractive interactions.

The analysis of charm in diffraction is performed by reconstructing $D^{*\pm}(2010)$ mesons in diffractive interactions. This analysis has been performed principally by members of the UK group and is nearing completion. A paper draft has been written and is waiting for the completion of the second analysis, after which the editorial board process can begin. This is expect to happen early in 2002. The definitive measurement of charm production in diffraction will be possible with upgrade data, due to the increased statistics and the improved non-diffractive background rejection.

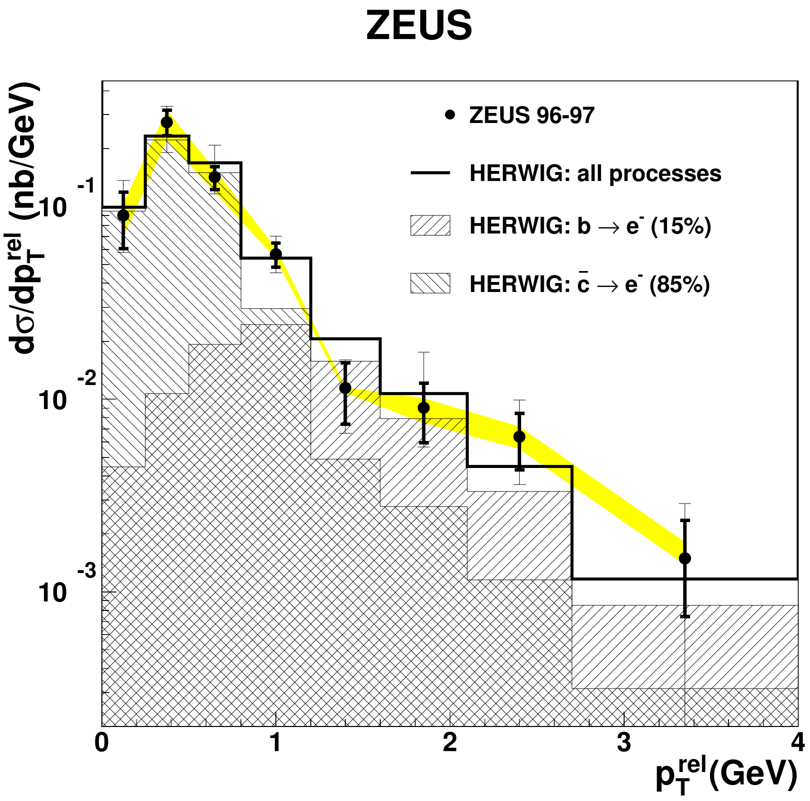

Figure 13: The transverse momentum of the electron relative to the jet axis, demonstrating the presence of beauty quarks

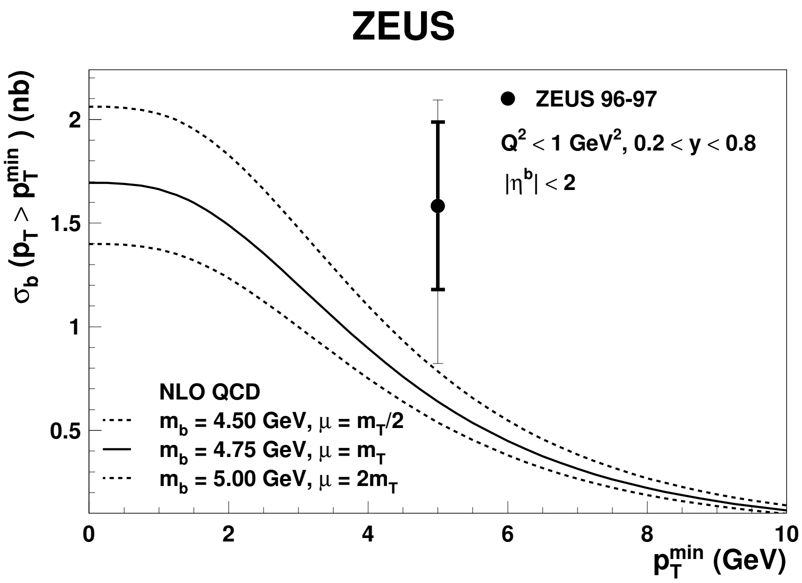

Figure 14: Extrapolated beauty quark cross section compared to NLO QCD predictions

5.3 QCD and the hadronic final state

5.3.1 Event Shapes

A recent revival of interest in the study of event shape measurements has been prompted by theoretical developments in the understanding of hadronisation or power corrections. Here, perturbative QCD calculations are extended into the region of low momentum transfers using approximations to higher-order graphs. At HERA, the Q^2 scale can be varied over four orders of magnitude enabling power corrections (proportional to $1/Q^p$, where p is the power) to be studied in detail. The data are compared to theoretical expectations for the power corrections, characterised by an effective coupling $\overline{\alpha}_0(\mu_I)$ specified at the infra-red matching scale $\mu_I \simeq 2$ GeV, and NLO pQCD calculations, determined by $\alpha_s(M_Z)$.
The Breit frame is where the exchanged gauge boson in DIS is purely space-like. Viewed in this frame, the incoming QPM quark is back-scattered with equal and opposite momentum $(Q/2)$. Event shapes have been measured in the direction of the struck quark, corresponding to the current region, which is directly analogous to one hemisphere of a purely time-like e^+e^- interaction. A series of event shape variables have been studied which have varying sensitivity to hadronisation/power corrections and are noted below. Thrust ($\tau = 1 - T_z$) and jet broadening (B) sum the longitudinal and transverse momenta, respectively, of individual particles along the photon axis. τ_c is also defined with respect to the reconstructed thrust axis, in order to compare directly with e^+e^-. Jet mass (ρ) and the C parameter sum the product of two particle momenta weighted by $1-\cos\theta_{ij}$ and $\sin^2\theta_{ij}$, respectively. These variables are each measured in the current region of the Breit frame and are scaled by the total visible energy (E_{vis}).
Mean values of these event shapes haves been measured by ZEUS [10] which can be interpreted theoretically via

$$\langle F \rangle = \langle F \rangle^{\rm pert} + \langle F \rangle^{\rm pow}$$

where

$$\langle F \rangle^{\rm pert} = c_{1,F}(x,Q) \cdot \alpha_s(Q) + c_{2,F}(x,Q) \cdot \alpha_s^2(Q)$$

with $c_{1,F}(x,Q)$ and $c_{2,F}(x,Q)$ being calculable coefficients of pQCD determined by the DISENT NLO program with renormalisation/factorisation scales set at $\mu_R = \mu_F = Q$. The power corrections are proportional to $1/Q$ with

$$\langle F \rangle^{\rm pow} = \mathcal{M}' \frac{a_F}{Q} \frac{16\mu_I}{3\pi} \left[\overline{\alpha}_0(\mu_I) - \alpha_s(Q) - \frac{23}{6\pi} \left(\ln \frac{Q}{\mu_I} + 1.45 \right) \alpha_s^2(Q) \right].$$

Here a_F is a calculable F-dependent coefficient and $\mathcal{M}' = 2\mathcal{M}/\pi \simeq 0.95$ is a two-loop level refinement to the calculations called the Milan factor.
Using the NLO calculation plus power correction approach described above, the mean event shape values versus Q are measured. Overall, a reasonable description of the data can be achieved, although the x-dependence of variables measured with respect to the photon axis, τ and B, is not well described. The major theoretical uncertainty is that due to the renormalisation scale.
The results of two-parameter fits to the ZEUS data both including and excluding the data at low x are shown in Figure 15. The correlation of $\overline{\alpha}_0(\mu_I)$ and $\alpha_s(M_Z)$ is high and negative for $\langle\tau\rangle$ but is less for other variables. In each case, the data for the means of τ, B, τ_C, C and ρ, are described reasonably well by the theory, with a value of the universal non-perturbative parameter $\overline{\alpha}_0(\mu_I)$ of $\simeq 0.5 \pm 20\%$ and a value of $\alpha_s(M_Z)$ close to the world average. There are, however, remaining theoretical uncertainties due to uncalculated higher-order x-dependent terms which appear to be especially significant for B. In conclusion, the theoretical approach works remarkably well and ongoing refinements will generate further insight into non-perturbative QCD mechanisms in the generation of hadronic final states at high energies. This analysis is currently in the final stages of the paper process and will lead to a publication soon.

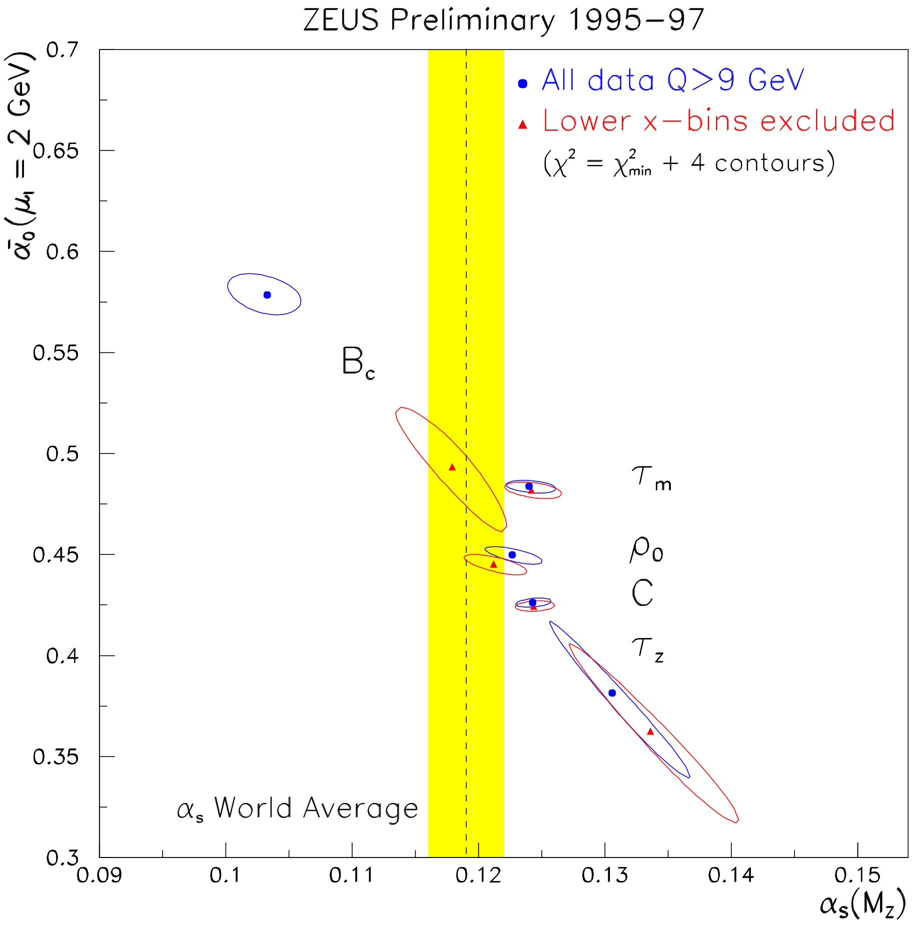

Figure 15: ZEUS preliminary contour plot of two-parameter fits of $\overline{\alpha}_0(\mu_I)$ and $\alpha_s(M_Z)$ to mean event shape variables. Two σ stat contours for fits both including and excluding the lower x data for τ, B, τ_C, ρ and C parameters are indicated.

5.3.2 Azimuthal Asymmetries

In the last report we presented the first observation of an azimuthal asymmetry between the lepton scattering plane and the hadron production plane for leading hadrons in the DIS hadronic centre-of-mass. This measurement has now been extended to study the angular assymmetry between between the lepton scattering plane and the jet production plane in inclusive dijet DIS events. This is illustrated compared to the DISENT NLO QCD calculation in figure 16 and shows clear evidence for a $\cos 2\phi$ contribution, a clear consequence of the underlying QCD.
Work is continuing [11] on the use of a neural network for the identification of quark and gluon jets in dijet events since their different helicity should yield distinct angular distrubtions and provide further insight into the QCD sub-process.

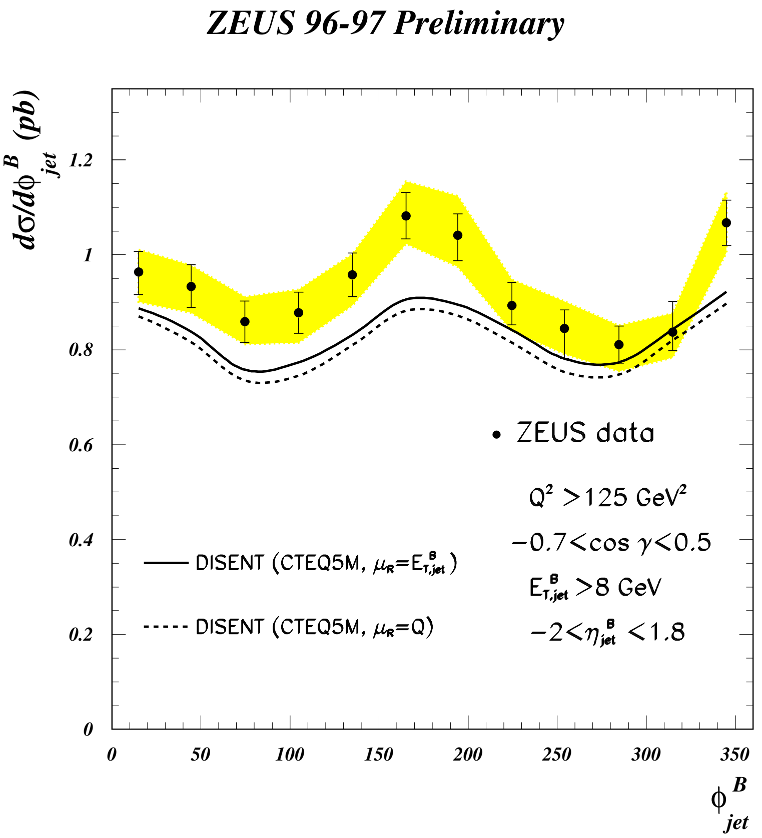

Figure 16: ZEUS preliminary jet cross section versus angle $\phi^B_{\rm jet}$ in the Breit frame in DIS compared to the DISENT NLO QCD calculation. The shaded area indicates the hadronic energy-scale uncertainty.

5.3.3 Jet Production

Our studies of jets in photon-proton collisions at HERA continue to give information on the hadronic "structure" of the photon, and UK groups continue to lead these analyses. In the last report we reported on our measurement [12] of the dynamics of three jet production with higher statistics than our previous measurement [13] and showing explicitly the effects of the colour of the incoming quarks and gluons – a fundamental test of the strong interaction. In addition we have recently published [14] precise data on dijet photoproduction at high E_T^{jet} including the dijet angular distributions

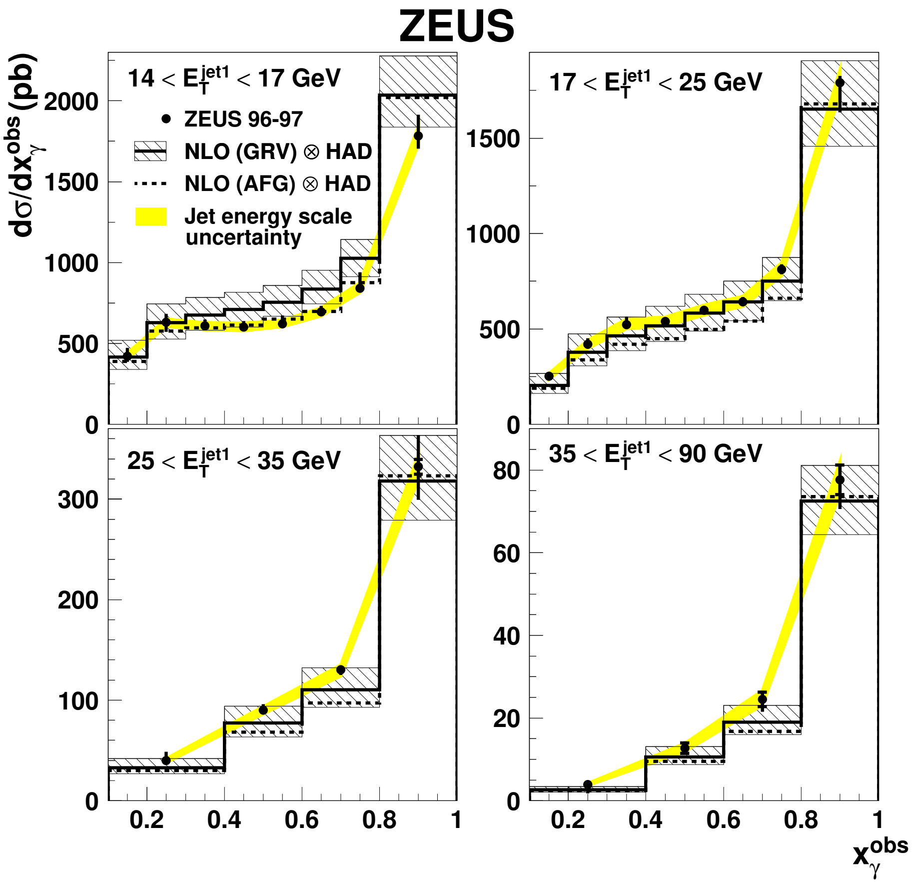

Figure 17: ZEUS jet cross sections compared to the NLO QCD calculation of Frixione and Ridolfi. The shaded areas for the data the theory prediction indicate the hadronic energy-scale uncertainty and the theoretical uncertainty respectively.

Although these angular distributions present a reassuring picture of jet photoproduction in that the dynamics are well described by QCD, there is growing evidence for a significant discrepancy in the rate of resolved photon interactions, with the data lying above the NLO QCD expectations by around 30%. We have measured cross sections differentially in η^{jet}, E_T^{jet} and x_γ^{OBS} – the fraction of the photon's momentum entering the hard subprocess. In all cases, although the direct-photon dominated high x_γ^{OBS} region agrees well with the theory, the resolved-photon dominated low-x_γ^{OBS} region shows an excess as may be seen in figure 17. The current evidence points to the photon structure as the source of this discrepancy – ZEUS is sensitive to the photon structure in a Q^2 region above that accessible by LEP. However the cross-section as a function of the cut on the transverse energy of the sub-leading jet (figure 18) suggests that the contribution from higher order processes may still be significant.

By extending the 3-jet measurement to study the inclusive 4-jet final state we are seeking to expand our understanding of the QCD sub-process at even higher orders and together with the extension of the 3-jet measurement to lower 3-jet invariant masses we are additionally able to search for signatures of multi-parton interactions – one of the leading uncertainties in the description of the jet final state at lower transverse energies.

Our recently published results [15] on dijet production at very high invariant mass, with higher precision than previously measured, allow the search for heavy resonances and new physics. Limits on $W^\pm$ and Z^0 production in the final state have been obtained and are $\sigma_{e^+p\to e^+Z^0X} <$ 5.9 pb and $\sigma_{e^+p\to e^+W^\pm X} < 7.4$ pb respectively. Although this limit on $W^\pm$ production is weaker than we obtain using the leptonic channel it provides a complementary picture from the hadronic final state. Limits on the production of new heavy resonances, coupling preferentially to the photon-gluon initial state, such as technicolour pseudo-Goldstone bosons [16], have also been obtained and are shown in figure 19.

5.3.4 Jet substructure

An important aspect of the description of the QCD final state in jet production, besides the overall event topology and rate of production, is in the description of structure of the jets themselves.

To study this we have measured the topology of the jets in photoproduction using both the mean jet-shape (the fraction, with respect to a cone of radius $R = 1$, of the jet energy within a cone of radius r) and the mean subjet multiplicity (the number of subjets within the jet for a varying distance scale, y_{cut}, used in the jet finding). The width of jets in QCD is sensitive both to the QCD coupling, α_S, and to the fragmentation of the partons in the jet due to differing colour factors of the primary parton.

The tendency for gluon initiated jets to be broader can be used to divide the sample into gluon enhanced (thick) and quark enhanced (thin) jets and to study the dynamics of the underying sub-process in more detail than possible in inclusive dijet production. Figure 20 shows the dijet angular distribution in the dijet centre-of-mass frame for samples enriched in gluon-gluon, quark-quark and gluon-quark jets.

In addition, by studying the behaviour of the mean jet shape as a function of the jet transverse energy the QCD coupling constant can be extracted in a complimentary way to that from the study the jet rates themselves. This is shown in figure 21; the values of α_s thus obtained providing a non-trivial test of the consistency of our understanding of the hadronic final state.

5.3.5 Virtual-photon structure

Both the behaviour of the pointlike virtual photon at high Q^2 and the hadronic structure of the low virtuality photon have been well studied. By looking at the production of dijet events as a function of the photon virtuality from very low to very high Q^2 we are additionally able to study the hadronic structure of the virtual photon.

Building on our previous analysis [17], we have made use of the higher luminosity now available to study the virtual photon structure triply differentially in photon vituality, mean dijet transverse energy squared and also $x_\gamma^{\rm OBS}$. This is illustrated in figure 23 compared to predictions using the SaS 1D [18] parametrisation of the virtual photon parton density functions.
As expected, the low $x_\gamma^{\rm OBS}$ cross-section falls faster with increasing Q^2 than the high $x_\gamma^{\rm OBS}$ cross-section and for $Q^2 > \bar{E_T}^2$, the data is well descibed by the Monte Carlo with no resolved contribution required. However, for $Q^2 < \bar{E_T}^2$, the direct contribution alone is not sufficient to describe the data and further, the low $x_\gamma^{\rm OBS}$ cross-section is not well described by the Monte Carlo at lower Q^2.

5.3.6 Strange hadron production

Strange particle production at HERA provides an important environment for the study of the hadron production mechanism in processes containing hadronic remnants and can yield important information of the universality of strange particle fragmentation functions.
By considering strange particle production in conjunction with the production of high E_T jets in the hadronic final state it is possible to study the dependence of the hadronization mechanism on the underlying kinematics of the perturbative QCD sub-process.
Using the large event sample now available at ZEUS we have measured [19] strange particle production both to higher precision, and more differentially that before. The cross-section for K_S^0 production in events with at least two high transverse energy jets is reasonably well described in shape by available Monte Carlo models. Figure 22 shows that while the Λ cross-section is reasonably well described in shape, normalizing the overall Monte Carlo cross-section to that given by the K_S^0 data over estimates the rate of Λ baryon production with respect to K_S^0 hadrons for HERWIG and slightly underestimates for PYTHIA.

5.3.7 Inclusive Prompt Photon Photoproduction

Further progress has been made in studying photoproduction processes in which a high-E_T photon is emitted. Such photons may be produced directly as part of the QCD hard scattering subprocess, and are known as prompt photons. In a first ZEUS paper [20] the observation of such processes was first confirmed at HERA and the basic characteristics of events with a prompt photon and a counterbalancing jet were established. In a more recent paper [21] the properties of inclusive prompt photons have been studied.
High energy photon production can be described as a sum of direct processes, dominated by the elastic scattering of the incoming photon off a quark in the proton, and resolved processes, in which the incoming photon is a source of partons which subsequently scatter. A source of photons which it is desirable to minimise comes from dijet processes in which a final state quark hard-radiates a photon, referred to radiative events. The requirement that the final-state photon be relatively isolated from other final-state particles reduces the radiative contribution and also neutral-meson backgrounds. The latter are finally subtracted off by means of signal-shape properties in the ZEUS barrel calorimeter.
We are currently extending this analysis to include the study of prompt photons in DIS events. This entire area of study will be further enhanced by the very much improved luminosities available after the HERA upgrade.
Figure 24 shows the effective transverse momentum of quarks within a proton, as they take part in direct photoproduction of a high transverse momentum prompt photon and a jet. Comparison is made with a variety of measurements from other experiments over a wide range of interaction energies, W. A consistent trend is observed.
A further study of prompt photon production in Deep Inelastic Scattering processes is underway.
INPUT NEEDED FROM WALCZAK

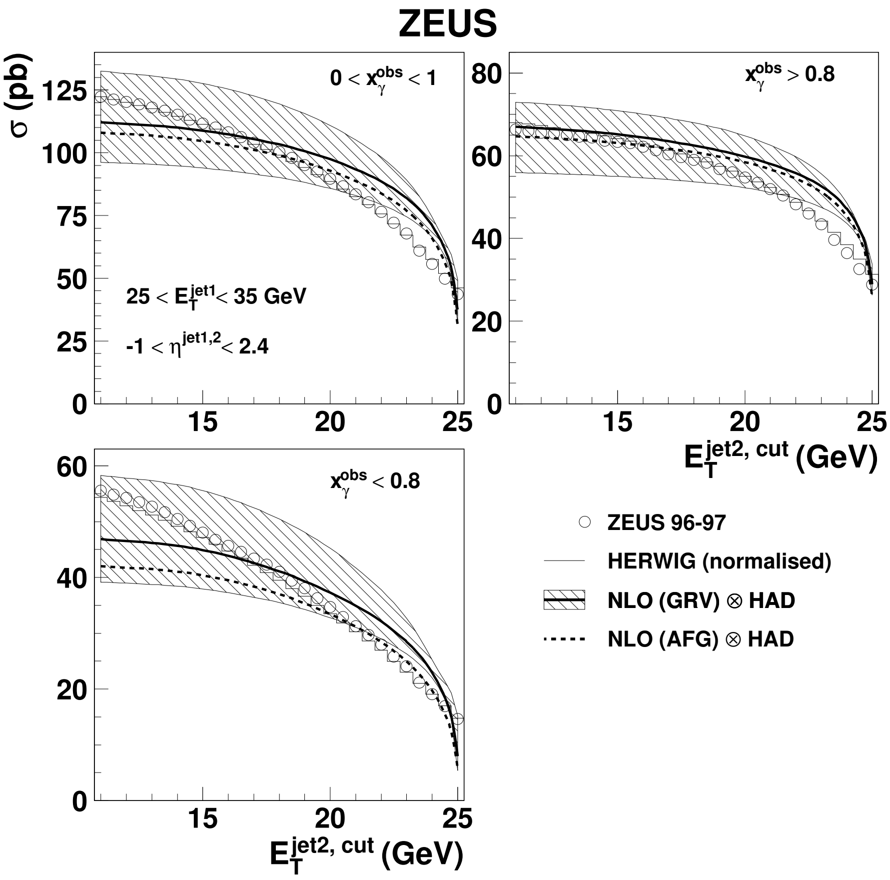

Figure 18: Total ZEUS dijet cross-sections for differing E_T cut on the sub-leading jet compared to HERWIG and the NLO QCD calculation of Frixione and Ridolfi. The shaded area indicates the NLO renormalisation scale uncertainty.

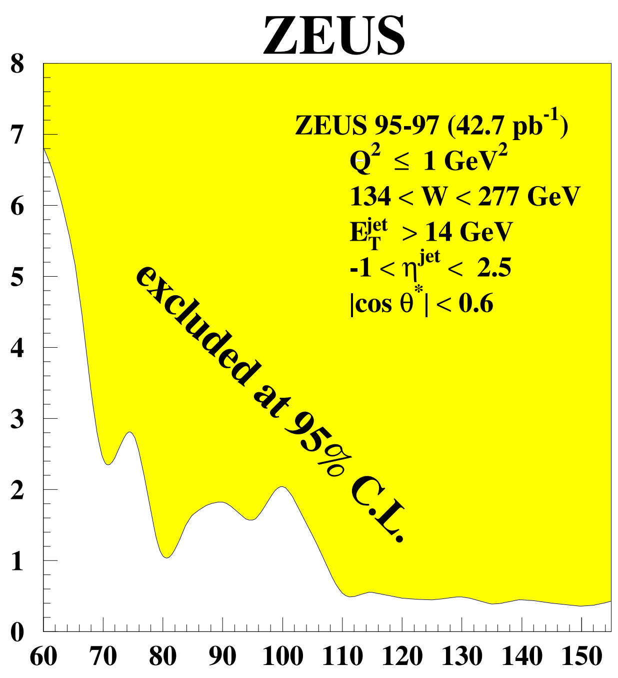

Figure 19: ZEUS excluded region of cross-section times branching ratio for new heavy resonances, $\mathcal{P}$, coupling preferentially to the photon-gluon initial state in the mass region 60< $M_{\mathcal{P}}$ <149 GeV.

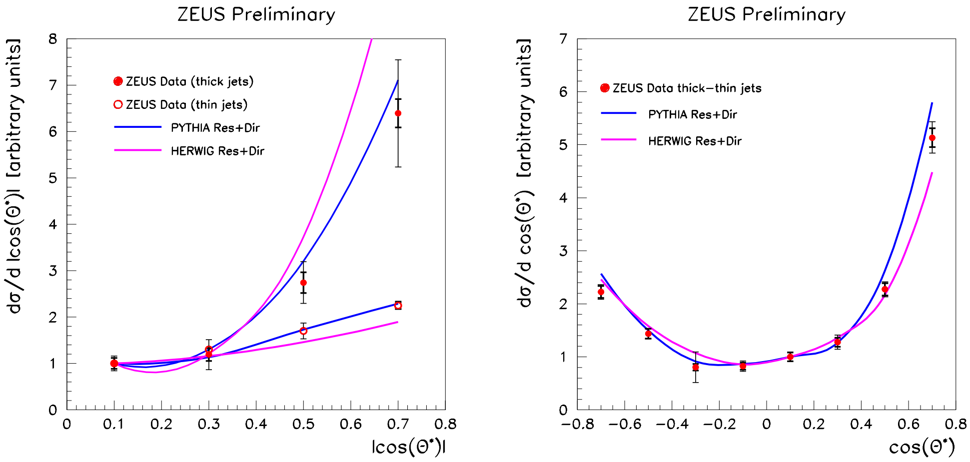

Figure 20: ZEUS preliminary jet cross-sections versus $\cos\theta^*$ compared to HERWIG and PYTHIA.

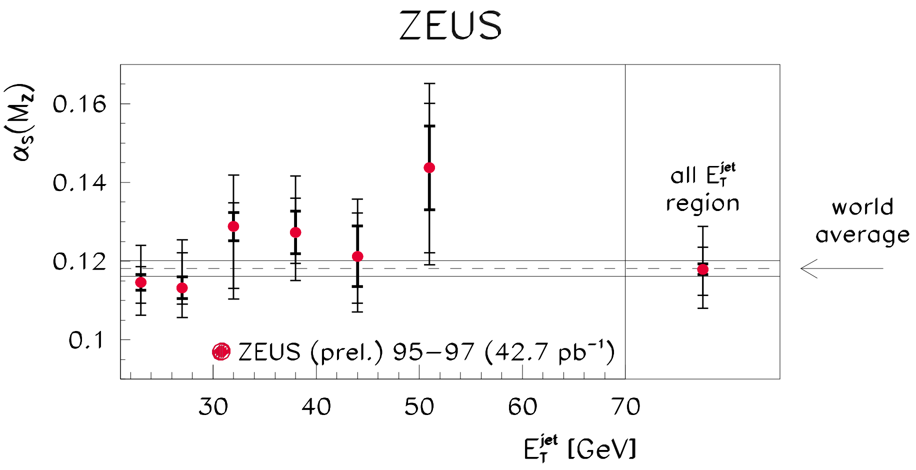

Figure 21: ZEUS preliminary values of α_S extracted from the jet-shape data.

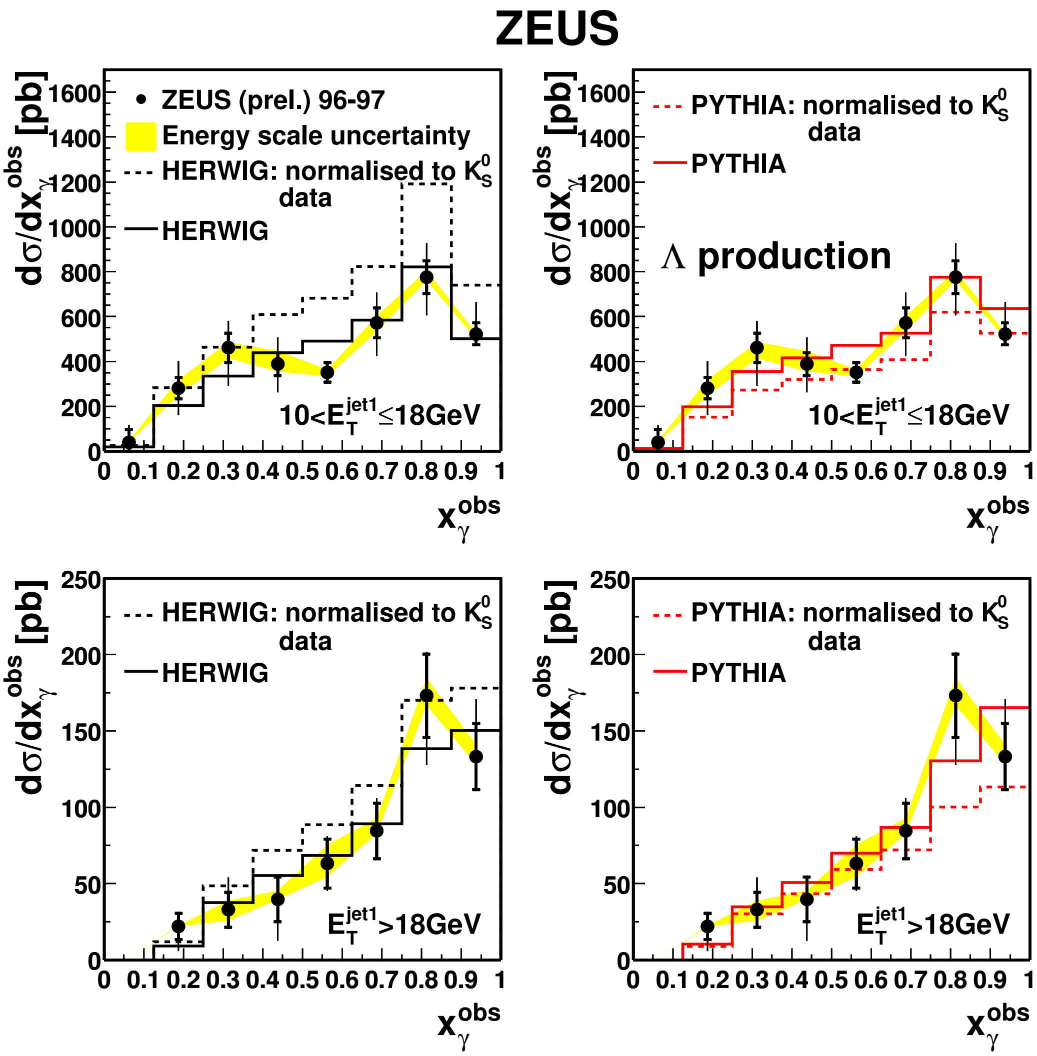

Figure 22: ZEUS preliminary cross-sections on Λ production for high transverse energy dijet photoproduction normalised both to the Λ data (solid) and to the K_S^0 data (dashed).

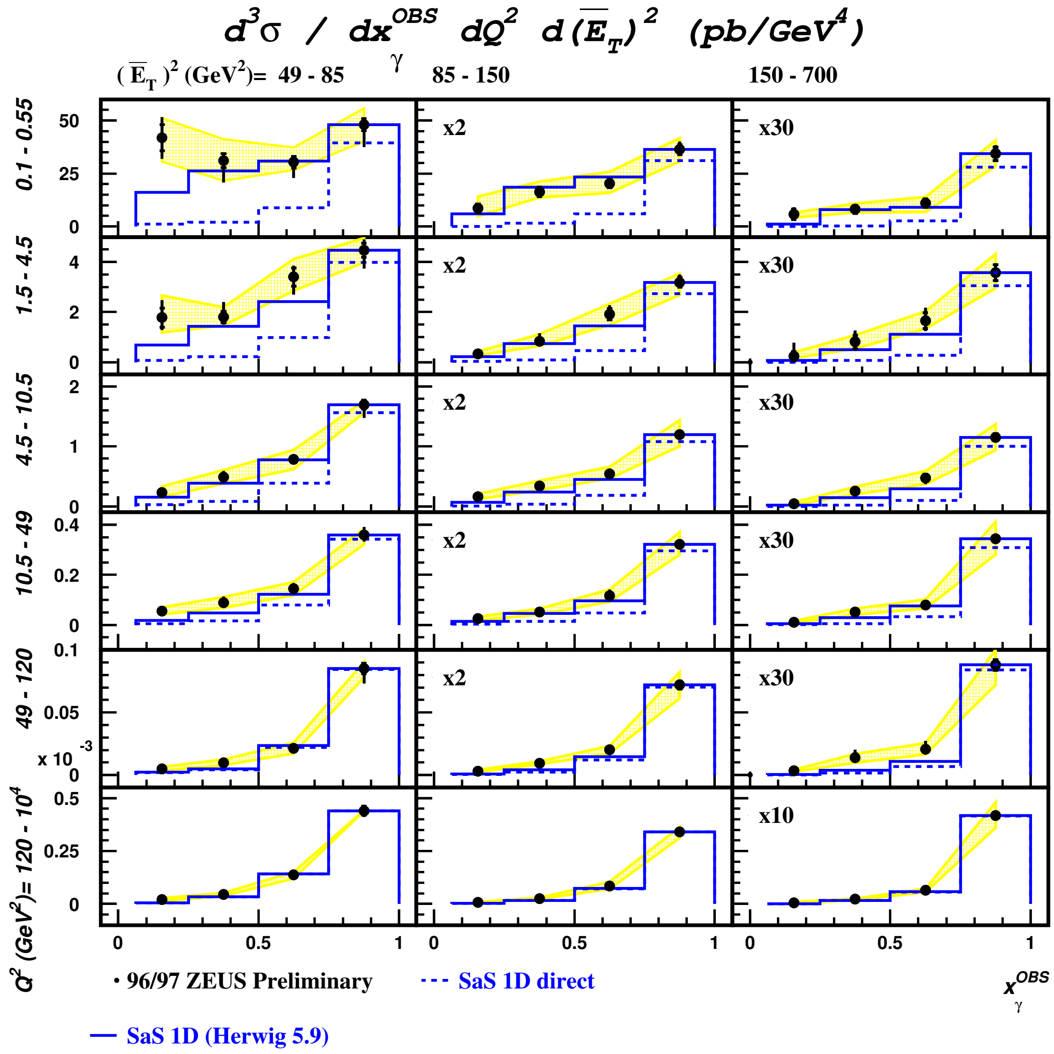

Figure 23: ZEUS preliminary dijet cross-sections, triply differential in Q^2, mean jet transverse energy squared and $x_\gamma^{\rm OBS}$ compared to HERWIG.

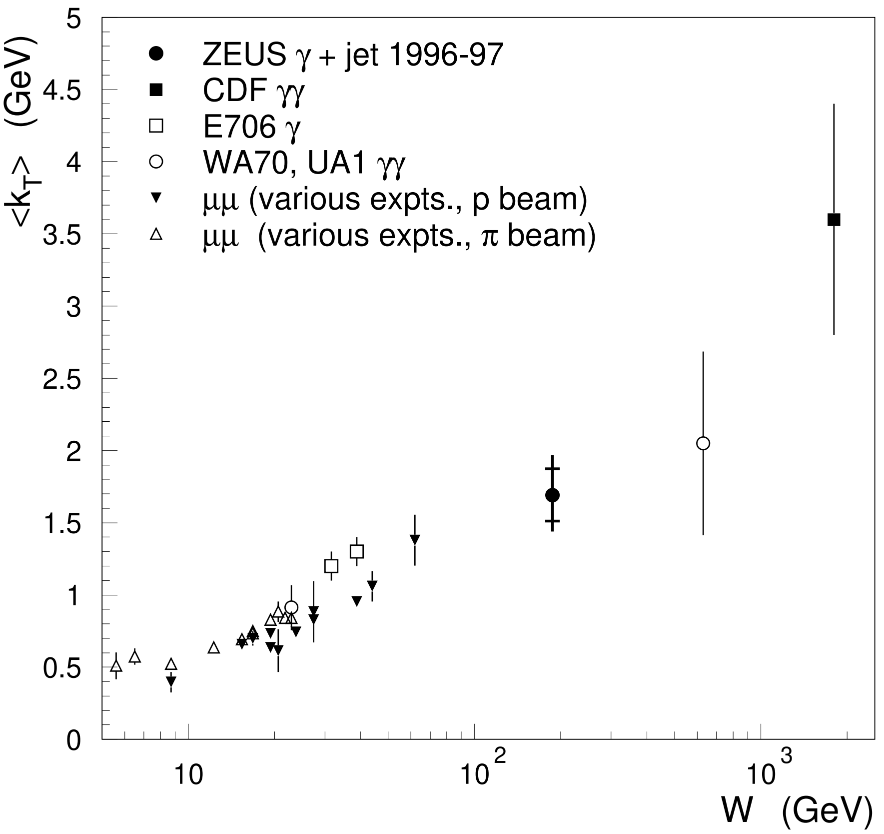

Figure 24: Effective transverse momentum of quarks within a proton, as they take part in direct photoproduction of a high transverse momentum prompt photon and a jet. Comparison is made with a variety of measurements from other experiments over a wide range of interaction energies W. A consistent trend is observed.

6 UK Ph D Theses

(Submitted during 2001.)

1. E.A. Heaphy (U.C.L., 2001) *Dijet Photoproduction and the Structure of the Photon*
2. G McCance (Glasgow, 2001) *Event Shapes and Power Corrections at HERA*
3. Info needed still from IC
4. B.J.West (U.C.L., 2001) *Charm and the Virtual Photon at HERA and a Global Tracking Trigger for ZEUS*

Talks on ZEUS and ZEUS-related physics given at major National or International Conferences not previously reported.

1. D S Bailey (Bristol) *Heavy Flavour Production at HERA*, New Trends in HEP, Yalta 22-29th Sept
2. N H Brook (Bristol) *Soft Multiparticle Production in DIS*, New Trends in HERA Physics, Ringberg 17-22 June
3. P J Bussey (Glasgow) *Prompt photons in photoproduction at HERA*, DIS2001, Bologna, 2001
4. J M Butterworth (ZEUS/UCL) *ZEUS Results and Status*, 51st DESY PRC 17 May, Open Session, DESY:
5. J E Cole (Brsitol) *Low x Physics at HERA*, XVIth Int. Workshop in HEP & Quantum Field Theory, Moscow 6-12th Sept
6. A M Cooper-Sarkar (Oxford) *Low x physics at HERA*, Invited talk at ISMD2000 Lake Balaton Hungary, to be published in the proceedings, hep-ph/0102151
7. A M Cooper-Sarkar (Oxford) *ZEUS NLO QCD fit*, Invited talk at EuroHEP01 Budapest Hungary, to be published in the proceedings, hep-ph/0110386
8. CM Cormack (RAL), *High Q^2 Physics at HERA*, XXVth Physics in Collision Conference, 28-30 June 2001, Seoul, Korea: PIC2001
9. A T Doyle (Glasgow) *Deep Inelastic Scattering*, CTEQ-IPPP Summer School, St Andrews, 2001
10. A T Doyle (Glasgow) *Event Shapes at HERA*, Low-x workshop, Oxford, 2000
11. B Foster (Bristol) *HERA II Physics*, DIS 2001 Bologna 27th April - 1st May
12. C Glasman (Glasgow) *Jet Production and QCD tests in DIS at HERA*, E.P.S. Int. Conf. on H.E. Physics, Budapest, 2001
13. R Hall-Wilton (now ZEUS/UCL) *Low-x and Diffraction* Lake Louise Winter Institute 18-24 Feb 2001, Alberta, Canada:
14. J C Hart (RAL) *Prompt Photons and DVCS*, Moriond Conference on QCD and High Energy Hadronic Interactions, 17-24 March 2001, Les Arcs, France: XXXVIth Rencontres de Moriond

15. E A Heaphy (ZEUS/UCL) *Jets and subjets* XXXI International Symposium on Multiparticle Dynamics 2001 1-7 Sept 2001, Datong, Shanxi Province, China: ISMD01
16. G McCance (Glasgow) *Event Shapes and Power Correction results from HERA*, Moriond Conf on QCD and related topics, Les Arcs, 2001
17. B J West (ZEUS/UCL) *Virtual photon strucure with charm* PHOTON 2001 2-7 Sept 2001, Ascona, Switzerland:
18. M Wing (Bristol) *Jets in DIS*, New Trends in HERA Physics, Ringberg 17-22 June
19. M Wing (Bristol) convenor, jets & inclusive hadron production. Summary of jets & inclusive hadron production, Photon 2001, Ascona, Switzerland 2-7th Sept
20. list needed from IC

ZEUS collaboration publications in 2001

Searches for excited fermions in ep collisions at HERA: DESY-01-132 (September 2001), submitted to Physics Letters B
Dijet Production in neutral current deep inelastic scattering at HERA: DESY-01-127 (August 2001) submitted to The European Physical Journal
Properties of hadronic final states in diffractive deep inelastic scattering at HERA: DESY-01-097 (July 2001) accepted by Phys. Rev. D - DG8170
Three-jet production in diffractive deep inelastic scattering at HERA: Physics Letters B 516 (2001) 3-4, pp 273-292
Measurement of the neutral current cross section and F_2 structure function for deep inelastic e^+p scattering at HERA: The European Physical Journal C 21 (2001) 3, pp 443-471
Multiplicity moments in deep inelastic scattering at HERA: Physics Letters B 510 (2001) 36-54
Study of the effective transverse momentum of partons in the proton using prompt photons in photoproduction at HERA: Physics Letters B 511 (2001) 19-32
Measurement of dijet production in neutral current deep inelastic scattering at high Q^2 and determination of α_s Physics Letters B 507 (2001) 70-88
Measurement of open beauty production in photoproduction at HERA: The European Physical Journal C 18 (2001) 625-637
Measurement of dijet cross sections for events with a leading neutron in photoproduction at HERA: Nuclear Physics B 596 (2001) 3-29
A search for resonance decays to $\bar{\nu}$-jet in e^+p scattering at HERA: Physical Review D 63 (2001) Issue 5, Article 052002

Papers by ZEUS-UK authors on ZEUS-related topics

1. P J Bussey (Glasgow) *Heavy Flavour Physics at HERA - a survey* DEST 01-197, hep-ph/0109254 45pp.

2. N H Brook (Bristol) and I O Skillicorn (Glasgow) *A comparison of momentum spectra in deep inelastic scattering with the modified leading-log approximation.* Phys. Lett. **B497** (2001) 55; Phys. Lett. **B479** (2000) 173.

References

[1] T. Matsushita et al., Optical alignment system for the ZEUS microvertex detector, Nucl. Instr. Meth. A 466 (2001) 383–389

[2] Proceedings of the workshop on 'Future Physics at HERA', eds. G. Ingelman, A de Roeck and R. Klanner, DESY 1996.

[3] ZEUS Collaboration, S.Chekanov et al, *Measurement of the neutral current cross-section and F_2 structure function for deep inelastic e^+p scattering at HERA* Eur. Phys. J. C21 (2001) 443.

[4] ZEUS Collaboration, J.Breitweg et al, *ZEUS Results on the Measurement and Phenomenology of F_2 at Low x and Low Q^2* Eur. Phys. J. C 7 (1999) 609.

[5] ZEUS Collaboration, J.Breitweg et al., *Measurement of the Proton Structure Function F_2 at Very Low Q^2 at HERA* Phys. Lett. B 487 (2000) 53.

[6] ZEUS Collaboration, J.Breitweg et al, *Measurement of High Q^2 Charged-Current e^+p Deep Inelastic Scattering Cross Sections at HERA* Eur. Phys. J. C 12 (2000) 411.

[7] ZEUS Collaboration, J. Breitweg et al., *Measurement of $D^{*\pm}$ production and the charm contribution to F_2 in deep inelastic scattering at HERA*, The European Physical Journal C 12 (2000) 35.

[8] ZEUS Collaboration, J. Breitweg et al., *Measurement of inclusive $D^{*\pm}$ and associated dijets cross sections in photoproduction at HERA*, The European Physical Journal C 6 (1999) 67.

[9] ZEUS Collaboration, J. Breitweg et al., *Measurement of open beauty production in photoproduction at HERA*, The European Physical Journal C 18 (2001) 625

[10] R. Waugh, Glasgow University PhD Thesis (1999); G. McCance, "Event Shapes at HERA", Moriond Proceedings ; G. McCance, Glasgow University Ph.D. Thesis (2000)

[11] E.Rodrigues; University of Bristol PhD Thesis (in preparation).

[12] E.A.Heaphy, *Three-jet Production at HERA*, Durham Workshop on Collider Physics, (Sept. 1999) *(published, proper citation)*; University College London PhD Thesis (2001).

[13] ZEUS Collaboration, J. Breitweg et al., Phys. Lett. B 443 (1998) 394-408.

[14] ZEUS Collaboration; *Dijet photoproduction and photon structure* to be published in Eur. Phys. J.(?).

[15] ZEUS Collaboration; *High mass dijets in photoproduction* to be published in Phys. Lett. **B**

[16] S.Weinberg; Phys. Rev. **D19** (1979) 1277; L.Susskind; Phys. Rev. **D20** (1979) 2619;

[17] ZEUS Collaboration; *virtual photon structure* Eur. Phys. J. (?); N.MacDonald, Glasgow University PhD Thesis (1999?).

[18] T.Sjöstrand and G.A.Schuler; Z. Phys. **C68** (1995) 607.

[19] S.Boogert; University of Oxford PhD Thesis (in preparation); Photon 2001 proceedings.

[20] ZEUS Collaboration, J. Breitweg et al., Phys. Lett. B 413 (1997) 201.

[21] ZEUS Collaboration, J. Breitweg et al., Phys. Lett. B 472 (2000) 175.